## PAPER

Check for updates

# Synthesis of Ru(II) and Os(II) photosensitizers bearing one 9,10-diamino-1,4,5,8-tetraazaphenanthrene scaffold†

Simon De Kreijger,[a] Emilie Cauët,[b] Benjamin Elias [ID] *[a] and Ludovic Troian-Gautier [ID] *[a,c]

The synthesis of eight Ru(II) and Os(II) photosensitizers bearing a common 9,10-disubstituted-1,4,5,8-tetraazaphenanthrene backbone is reported. With Os(II) photosensitizers, the 9,10-diNH$_2$-1,4,5,8-tetraazaphenanthrene could be directly chelated onto the metal center *via* the heteroaromatic moiety, whereas similar conditions using Ru(II) resulted in the formation of an *o*-quinonediimine derivative. Hence, an alternative route, proceeding *via* the chelation of 9-NH$_2$-10-NO$_2$-1,4,5,8-tetraazaphenanthrene and subsequent ligand reduction of the corresponding photosensitizers was developed. Photosensitizers chelated *via* the polypyridyl-type moiety exhibited classical photophysical properties whereas the *o*-quinonediimine chelated Ru(II) analogues exhibited red-shifted absorption (520 nm) and no photoluminescence at room temperature in acetonitrile. The most promising photosensitizers were investigated for excited-state quenching with guanosine-5′-monophosphate in aqueous buffered conditions where reductive excited-state electron transfer was observed by nanosecond transient absorption spectroscopy.

## Introduction

Transition metal complexes based on Ru(II) and Os(II) photosensitizers have numerous applications in fields that include photoredox catalysis,[1–3] luminescence cellular imaging,[4–7] photodynamic therapy and other biomedical applications,[8–12] as well as solar energy conversion.[13–19] Despite efforts to move towards earth abundant photosensitizers,[20–23] these applications and research efforts still rely heavily on photosensitizers based on scarcer transition metals due to their robustness, tuneable excited-state lifetime and redox potentials, as well as controlled excited-state localization.[24,25] A common interest however, for many photosensitizers, earth abundant and rare, is the development of ligands with extended π-systems or with the ability to bridge a second metal center.[26–38] For example, in biomedical applications, intercalation within DNA or photoreaction with DNA bases was made possible with transition metal complexes (Ru, Rh, Os) carrying extended ligands such as TPPHZ (tetrapyrido[3,2-*a*:2′,3′-*c*:3″,2″-*h*:2‴,3‴-*j*]phenazine), dppz (dipyrido[3,2-*a*:2′,3′-*c*]phenazine), PHEHAT (1,10-phenanthrolino[5,6-*b*]-1,4,5,8,9,12-hexaazatriphenylene) or TAPHAT (1,4,5,8-tetraazaphenanthrene[9,10-*b*]-1,4,5,8,9,12-hexaazatriphenylene).[27,39–43] The structure of these ligands are presented in the ESI.† Such complexes were also used in artificial photosynthesis[44–51] and several binuclear photosensitizers based on the bridging TPPHZ ligand have also been developed for bio-imaging purposes.[4–6] The photoreactivity of such complexes could be further tuned by the use of different ancillary ligands that, for example, possess a strong π-accepting character, such as 1,4,5,8-tetraazaphenanthrene (TAP) or 1,4,5,8,9,12-hexaazatriphenylene (HAT). Such photosensitizers can react with Guanine, *i.e.* the DNA base with the most reducing power, to form the corresponding mono-reduced complex and the oxidized guanine *via* photoinduced electron transfer.[52–59]

The TPPHZ ligand has been extensively used in the field of hydrogen photoproduction with the development of photosensitizers such as [Ru(dtb)$_2$(TPPHZ)MX$_2$]$^{2+}$, where M is either Pt or Pd, X is Cl or I, and dtb is 4,4′-$^t$Bu-2,2′-bipyridine.[35–37] Light excitation of these photosensitizers leads to an initial electron transfer from the Ru(II) centre to the bridging ligand, followed by the activation of the catalytic centre (M). The Ru(II) centre is usually regenerated by electron transfer from a sacrificial elec-

*[a] UCLouvain, Institut de la Matière Condensée et des Nanosciences (IMCN), Molecular Chemistry, Materials and Catalysis (MOST), Place Louis Pasteur 1/L4.01.02, B-1348 Louvain-la-Neuve, Belgium. E-mail: Benjamin.Elias@uclouvain.be, Ludovic.Troian@uclouvain.be*

*[b] Spectroscopy, Quantum Chemistry and Atmospheric Remote Sensing (CP 160/09), Université libre de Bruxelles (ULB), 50 av. F. D. Roosevelt, CP160/09, B-1050 Brussels, Belgium*

*[c] Wel Research Institute, Avenue Pasteur 6, 1300 Wavre, Belgium*

†Electronic supplementary information (ESI) available: $^1$H NMR and HR-MS characterization, electrochemistry and DFT calculations. See DOI: https://doi.org/10.1039/d4dt01077a

tron donor reagent present in solution such as triethylamine or triethanolamine. This light-activated process is repeated a second time to fully activate the secondary metal centre, which can then perform proton reduction to form molecular hydrogen. Similar approaches are used for $CO_2$ reduction, as well as for the development of photocathode or photoanode materials.[15,60–66] A general pattern in the photocatalysis approach is to connect a photosensitizer and catalytic centre *via* a bridging ligand. This allows for efficient electron or hole transfer and subsequent long-lived charge separated state, as well as the modification of the associated redox potential, which can tune the range and efficiency of possible transformations.[67] Hence, the development of new bridging structures to funnel electrons between metal centres is still highly relevant.

Here, we focused on the development of a series of photosensitizers bearing a common ligand scaffold, 9,10-diNH$_2$-1,4,5,8-tetraazaphenanthrene (Fig. 1).[68–73] The 1,4,5,8-tetraazaphenanthrene (TAP) offers similar redox potential as the prototypical 2,2′-bipyrazine ligand while the inclusion of the diamino functionality would allow for the straightforward development of a series of bridging ligands, through condensation with *o*-diones, such as 1,10-phenanthroline-5,6-dione, for example. We found that 9,10-diNH$_2$-1,4,5,8-tetraazaphenanthrene could be directly chelated onto Os(II) centres but that,

with Ru(II), the chelation efficiency strongly depended on the ancillary ligands. When 1,10-phenanthroline ancillary ligands were used, chelation of 9,10-diNH$_2$-1,4,5,8-tetraazaphenanthrene led to the formation of two photosensitizers; one where the diamine ligand is chelated *via* the polypyridyl-type backbone and a second one where the ligand is coordinated as an *o*-quinonediimine. Such coordination scaffold has already been reported in the literature, amongst others by A. B. P. Lever.[74–78] This led to drastically different ground and excited-state properties, as described herein.

## Experimental

Acetonitrile 99.9% (VWR), dichloromethane 99.9% (stabilized with about 0.002% of 2-methylbut-2-ene, VWR), diethyl ether 99.9% (VWR), ethanol absolute 99.9% (VWR), methanol 99.9% (VWR), ethylene glycol ≥ 99.5% (Roth), cyclohexane 99.9% (VWR), acetone 99.9% (VWR), chloroform ≥ 99.8% (VWR), 1,4-dioxane 99.8% (Sigma-Aldrich), hydrochloric acid 37% (VWR), acetic acid glacial ≥ 99.7% (Fischer Chemical), Celite (Roth) aluminium oxide, for chromatography, neutral, Brockmann I, 40–300 μm, 60 Å (Thermo Fischer), silica gel 60 Å for flash column chromatography, 40–63 μm (ROCC), sephadex LH-20
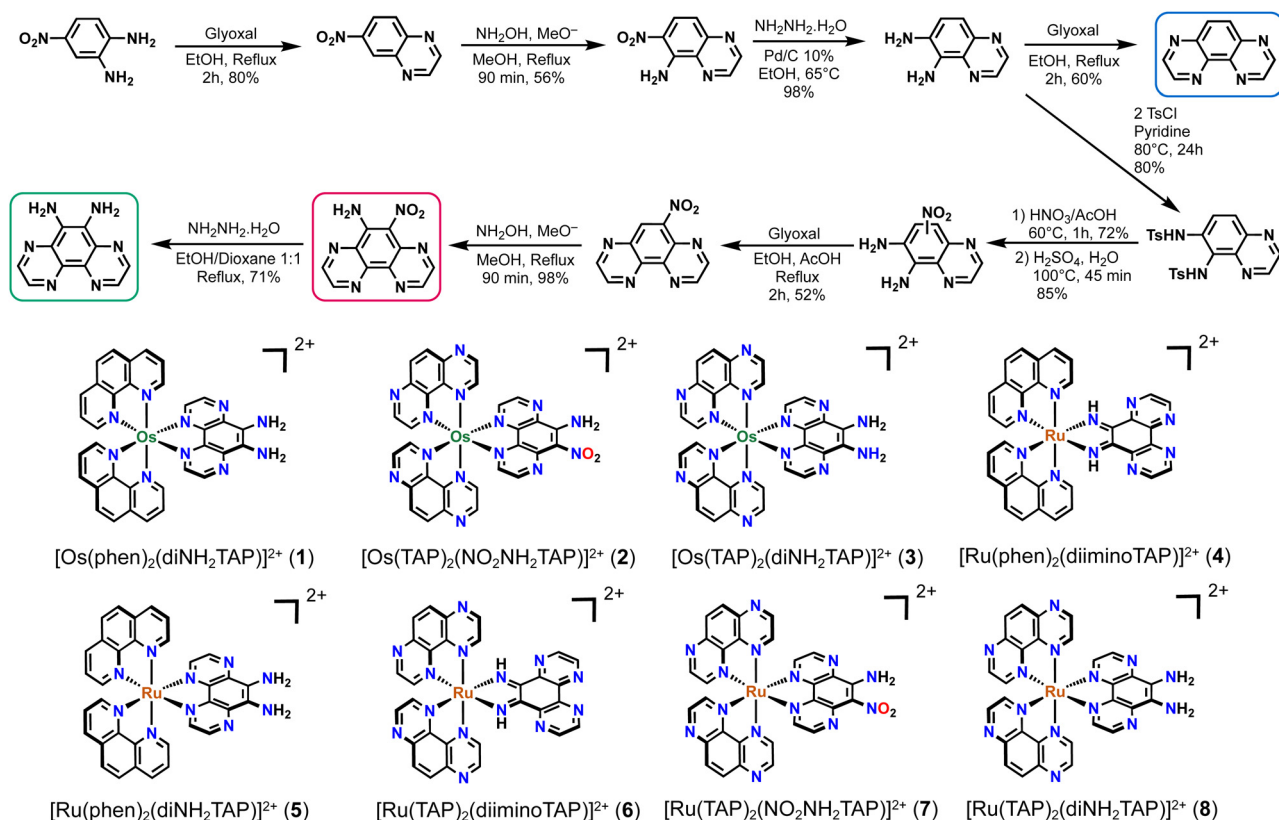


**Fig. 1** Synthesis scheme of 1,4,5,8-tetraazaphenanthrene (TAP), 9-amino-10-nitro-1,4,5,8-tetraazaphenanthrene (NO$_2$NH$_2$TAP) and 9,10-diamino-1,4,5,8-tetraazaphenanthrene (diNH$_2$TAP) alongside the structures of the eight photosensitizers reported in the present study: [Os(phen)$_2$(diNH$_2$TAP)]$^{2+}$ (**1**), [Os(TAP)$_2$(NO$_2$NH$_2$TAP)]$^{2+}$ (**2**), [Os(TAP)$_2$(diNH$_2$TAP)]$^{2+}$ (**3**) [Ru(phen)$_2$(diiminoTAP)]$^{2+}$ (**4**), [Ru(phen)$_2$(diNH$_2$TAP)]$^{2+}$ (**5**), [Ru(TAP)$_2$(diiminoTAP)]$^{2+}$ (**6**), [Ru(TAP)$_2$(NO$_2$NH$_2$TAP)]$^{2+}$ (**7**), and [Ru(TAP)$_2$(diNH$_2$TAP)]$^{2+}$ (**8**).

(GE Healthcare), sodium hydroxide ≥ 98.0% (Roth), pyridine ≥ 99% (VWR), *p*-toluenesulfonyl chloride ≥ 99.0% (Acros Organics), hydrazine hydrate 50–60% (Sigma-Aldrich), palladium (10%) on activated carbon (Chimet), (+)-sodium ʟ-ascorbate 99.0% (Acros Organics), guanosine 5′-monophosphate disodium salt hydrate ≥ 99.0% (TCI), tris-(hydroxymethyl)-aminomethane hydrochloride ≥ 99.5% (VWR), glyoxal 40 wt% in water (Acros Organics), sodium in kerosene ≥ 99.8% (Sigma Aldrich), hydroxylamine hydrochloride ≥ 99.0% (Acros Organics), ammonia 25% solution (Roth) and 4-nitro-*o*-phenylenediamine 98% (Acros Organics) were purchased from commercial suppliers and used as received. Water was purified by a Millipore Milli-Q system.

### UV-Vis spectroscopy

UV–vis absorption spectra were recorded on an Agilent Cary 60 spectrophotometer in a 1 cm path length quartz cuvette.

### Microwave synthesis

Microwave (MW) syntheses were performed on a Milestone MicroSYNTH labstation under magnetic stirring. Typically, the conditions allowed the vessels to reach the desired temperature in 5 minutes and the vessels were held at the desired temperature for the indicated period.

### Stern–Volmer experiments

A photosensitizer stock solution with an absorbance of ∼0.1 to ∼0.2 at the excitation wavelength was prepared in the tris–HCl solvent mixtures. The guanosine 5′-monophosphate disodium hydrate salts were diluted with 2 mL of the photosensitizer stock solution. 3 mL of the stock solution were transferred to a quartz cuvette equipped with a 24/40 joint. The guanosine 5′-monophosphate disodium salt hydrate quencher was then gradually added to the cuvette. This allowed to increase the concentration of quencher while keeping the concentration of photosensitizer constant. The excited-state quenching was monitored by time-resolved spectroscopy using the Edinburgh Instruments FS5 Spectrofluorometer equipped with a time-correlated single photon counting module. The decrease of excited-state lifetime or photoluminescence is directly related to the concentration of quencher and the respective Stern–Volmer plots were extrapolated using eqn (1). The quenching rate constant ($k_q$) was then determined by dividing the slope by the initial lifetime without any quencher, determined for each experiment.

$$\frac{\sum^{(PLI_0)}}{\sum^{(PLI)}} = \frac{\tau_0}{\tau} = 1 + K_{SV}[Q] = 1 + k_q \tau_0 [Q] \quad (1)$$

### Transient absorption spectroscopy

Nanosecond transient absorption measurements were recorded on previously described setup.[79] Briefly a LP980-K spectrometer from Edinburgh Instruments equipped with an iCCD detector from Andor (DH320T). The excitation source was a tuneable Nd:YAG Laser NT342 Series from EKSPLA. The third harmonic (355 nm) at 100 mJ was directed into an optical parametric oscillator (OPO) to enable wavelength tuning starting from 410 nm. The laser power was then attenuated to reach appreciable signal/noise and the integrity of the samples was verified by UV–Vis measurements. The LP980-K is equipped with a symmetrical Czerny-Turner monochromator. For single wavelength absorption changes, an 1800 g mm$^{-1}$ grating, blazed at 500 nm is used, which affords wavelength coverage from 200 to 900 nm. For spectral mode (iCCD), a 150 g mm$^{-1}$ grating, blazed at 500 nm is used, offering a wavelength coverage of 540 nm over the full wavelength range extending from 250 to 900 nm. Single wavelength absorption changes were monitored using a PMT LP detector (Hamamatsu R928) which covers the spectral range from 185 to 870 nm. The probe was a 150 W ozone-free xenon short arc lamp (OSRAM XBO 150 W/CR OFR) that was pulsed at the same frequency of the laser. The excitation wavelength depended on the photosensitizers but in all cases the concentration at the excitation wavelength was adjusted to reach absorbance values between 0.3 and 0.5. All measurements were performed in argon-purged Tris-HCl buffer (50 mM, pH 7.4) at room temperature. An average of 30 to 90 scans per measurement was used.

### Density functional theory calculations

The computational methodology is based on Density Functional Theory (DFT) and time dependent DFT (TD-DFT) methods. All calculations were performed using the Gaussian 16 computational chemistry package while applying default procedures, integration grids, algorithms and parameters.[80] As a first step, the equilibrium geometries of the singlet state of the Ru(ɪɪ) complexes [(Ru(phen)$_2$(diNH$_2$TAP)]$^{2+}$, [Ru(TAP)$_2$(diNH$_2$TAP)]$^{2+}$, [Ru(phen)$_2$(diiminoTAP)]$^{2+}$ and [Ru(TAP)$_2$(diiminoTAP)]$^{2+}$) were optimized in acetonitrile using the integral equation formalism model (IEFPCM).[81] These calculations were performed using the hybrid B3LYP exchange–correlation functional.[82–84] The 6-31+G(d,p) basis set[85,86] was used for the C, N and H atoms while the def2-SVP relativistic effective core potential and associated basis set was employed to describe the Ru atoms.[87,88] The harmonic vibrational frequencies of each complex have been calculated with the same level of calculation, and it has been checked that all structures correspond to true minima of the potential energy surface. Cartesian coordinates for all atoms in optimized structures of the complexes are provided (Tables S1–S4†).

Time-dependent DFT (TD-DFT) method was employed to investigate the excited-state electronic structure of each of the complexes. The first lowest-lying excited states of the complexes at their ground-state singlet geometries have been evaluated within the vertical TD-DFT approximation, using the level of theory B3LYP/6-31+G(d,p)/def2-SVP. The modelling of solvent effects (here acetonitrile) has been included through the IEF-PCM model. To be able to discuss the excited states characters, it was favourable to analyse the frontier orbitals.[89] However, because the canonical orbitals created by the DFT method did not represent well the excited state transitions

(due to the fact that, in many cases, interacting configurations are present), the natural transition orbitals (NTO's) have been used. The NTO's can be interpreted in a similar sense as the DFT orbitals, only that they are specifically adapted to the excited state of interest.

## Synthesis

**6-Nitroquinoxaline.** 128 mL of 40% glyoxal was added in a dropwise fashion to a hot solution of 4-nitro-1,2-diaminobenzene (92.2 g, 602 mmol) in 800 mL of absolute ethanol. The thick solution was mechanically stirred at refluxed for two hours. The progress of the reaction was monitored by TLC (SiO$_2$, cyclohexane/acetone 7 : 3). Once the reaction was complete, the solution was cooled down to room temperature then in an ice bath. The precipitate was collected by filtration and the solid was subsequently rinsed with cold methanol to afford 6-nitroquinoxaline as a yellow solid (84.4 g, 80%). **1H NMR** (300 MHz, CDCl$_3$) $\delta$ 9.08–8.99 (m, 3H), 8.57 (dd, $J$ = 9.2, 2.5 Hz, 1H), 8.29 (d, $J$ = 9.2 Hz, 1H). NMR shifts agreed with the reported values.[90]

**5-Amino-6-nitroquinoxaline.** A sodium methanolate solution was prepared by adding small portions of sodium (29.2 g, 1.27 mol) to 1.2 L of methanol. After reaction of the metallic sodium, hydroxylamine hydrochloride (37.6 g, 540 mmol) previously dissolved in 600 mL of methanol was added. After settling, the sodium chloride was filtered off and the filtrate poured into a suspension of 6-nitroquinoxaline (60.0 g, 344 mmol) in 1.2 L of methanol, which was then refluxed and stirred. The reaction medium quickly turned black. Reflux was maintained and the progress of the reaction monitored by TLC (10 mL CHCl$_3$ with 2 to 5 drops of ammonia). Once the starting product disappeared, the reaction medium was cooled down to room temperature. The solution was filtered, and the precipitate washed with cold methanol to yield 5-amino-6-nitroquinoxaline as a brown powder (36.4 g, 56%). **1H NMR** (300 MHz, CDCl$_3$) $\delta$ 8.97 (d, $J$ = 1.9 Hz, 1H), 8.75 (d, $J$ = 1.9 Hz, 1H), 8.40 (d, $J$ = 9.7 Hz, 1H), 7.27 (d, $J$ = 9.7 Hz, 3H). NMR shifts agreed with the reported values.[90]

**5,6-Diaminoquinoxaline.** 122 mL of 98% hydrazine hydrate were added dropwise to a suspension of 5-amino-6-nitroquinoxaline (92.5 g, 485 mmol) and 8.9 g of 10% Pd/C in 3.6 L of ethanol. The reaction medium was heated to 65 °C and the reduction was monitored by TLC (SiO$_2$, CHCl$_3$/acetone 8 : 2). After reaction, the catalyst was removed by filtration through Celite. The red solution was evaporated under reduced pressure. The recovered solid was dried under vacuum to yield 5,6-diaminoquinoxaline as a red powder (76.1 g, 98%). **1H NMR** (300 MHz, CDCl$_3$) $\delta$ 8.62 (dd, $J$ = 1.9 Hz, 2H), 7.50 (d, $J$ = 8.8 Hz, 1H), 7.32–7.22 (m, 1H), 4.39 (s, 2H), 3.77 (s, 2H). NMR shifts agreed with the reported values.[90]

**1,4,5,8-Tetraazaphenanthrene.** 44 mL of a 40% aqueous glyoxal solution was added dropwise to a hot solution of 5,6-diaminoquinoxaline (33.1 g, 206 mmol) in 350 mL of ethanol. The solution was then refluxed and monitored by TLC (SiO$_2$, CHCl$_3$/acetone 9 : 1). After reaction, the reaction medium was cooled down to room temperature and filtered. The precipitate

was purified by silica gel column chromatography (CH$_2$Cl$_2$/acetone 80 : 20 to 50 : 50). The solvents were removed to recover 1,4,5,8-tetraazaphenanthrene as a white cotton-like solid (22.8 g, 60%). **1H NMR** (300 MHz, DMSO-d$_6$) $\delta$ 9.23 (d, $J$ = 2.0 Hz, 2H), 9.20 (d, $J$ = 2.0 Hz, 2H), 8.37 (s, 2H). NMR shifts agreed with the reported values.[90]

**5,6-Bis(*N-p*-toluenesulfonamido)quinoxaline.** To a stirred solution of 5,6-diaminoquinoxaline (55.5 g, 345 mmol) in 200 mL pyridine, *p*-toluenesulfonyl chloride (132.4 g, 696 mmol) was added in portions. The mixture was then refluxed for 24 hours. After reaction, the reaction medium was cooled down to room temperature and poured over 2.8 L of ice-cold water containing 106 mL of hydrochloric acid (37%), allowing the compound of interest to precipitate as a brown powder. The solid was then washed four times with 800 mL of a water/HCl solution (28 : 1), with ethanol (800 mL) and diethyl ether (800 mL). The final product was dried under vacuum to yield 5,6-bis(*N-p*-toluenesulfonamido)quinoxaline as a beige solid (129.1 g, 80%). **1H NMR** (300 MHz, CDCl$_3$) $\delta$ 9.15 (s, 1H), 8.61 (d, $J$ = 1.9 Hz, 1H), 8.34 (d, $J$ = 1.9 Hz, 1H), 8.24 (d, $J$ = 9.4 Hz, 1H), 7.89 (d, $J$ = 9.4 Hz, 1H), 7.85–7.76 (m, 2H), 7.55 (s, 1H), 7.37–7.28 (m, 2H), 7.33–7.18 (m, 2H), 6.94–6.85 (m, 2H), 2.36 (s, 3H), 2.19 (s, 3H). NMR shifts agreed with the reported values.[69]

**5,6-Bis(*N-p*-toluenesulfonamido)-8(7)-nitroquinoxaline.** To a suspension of 5,6-bis(*N-p*-toluenesulfonamido)quinoxaline (7.0 g, 15.2 mmol) in 60 mL of acetic acid maintained at 60 °C, approximately one third of a nitrating mixture prepared from fuming nitric acid (1 mL) and glacial acetic acid (10 mL) was added. Shortly after the first addition, the dissolution of the product was observed. Over time, a brown precipitate began to appear. Finally, the rest of the nitrating mixture was added, and the reaction was refluxed for 1 hour. After reaction, the medium was brought to 0 °C and the precipitate was collected by filtration and washed with acetic acid and water. 5,6-Bis(*N-p*-toluenesulfonamido)-8(7)-nitroquinoxaline was obtained as a beige solid (5.56 g, 72%). **1H NMR** (300 MHz, CDCl$_3$) $\delta$ 9.35 (s, 1H), 8.80 (d, $J$ = 1.8 Hz, 1H), 8.74 (s, 1H), 8.51 (d, $J$ = 1.8 Hz, 1H), 7.90–7.83 (m, 2H), 7.80 (s, 1H), 7.41–7.35 (m, 2H), 7.31–7.27 (m, 2H), 7.01–6.95 (m, 2H), 2.39 (s, 3H), 2.23 (s, 3H). NMR shifts agreed with the reported values.[69]

**5,6-Diamino-8(7)-nitroquinoxaline.** The nitro compound (50.0 g, 97.4 mmol) was dissolved in 155 mL of concentrated sulphuric acid, containing 8 mL of water, and heated to 100 °C. The mixture was stirred for 50 minutes at this temperature before being poured onto ice. The solution was then brought to a pH of 9 by addition of NaOH (12 M). The dark red precipitate was filtered, washed with water and dried under vacuum to afford 5,6-diamino-8(7)nitroquinoxaline (17.0 g, 85%). **1H NMR** (300 MHz, CDCl$_3$) $\delta$ 8.90 (d, $J$ = 1.9 Hz, 1H), 8.80 (d, $J$ = 1.9 Hz, 1H), 7.62 (s, 1H), 7.50 (s, 2H), 4.51 (s, 2H). NMR shifts agreed with the reported values.[69]

**9-Nitro-1,4,5,8-tetraazaphenanthrene.** 5,6-Diamino-8(7)nitroquinoxaline (35.8 g, 174 mmol) was added to a mixture of 3.5 L ethanol and 130 mL acetic acid and refluxed. Glyoxal (79 mL glyoxal 40%) was then added dropwise, and reflux was

maintained for 3 hours. The mixture was concentrated to a volume of approximately 150 mL. Water was then added and neutralisation with ammonia resulted in the recovery of a brown precipitate, which was recovered by filtration. The solid was washed with acetone at room temperature and then with 1 L of hot acetone. The filtrate was recovered, and the acetone evaporated. The product obtained was then purified by a silica gel chromatography column (CHCl$_3$/acetone, 8 : 2) to yield the title compound as a beige solid (20.5 g, 52%). **$^1$H NMR** (300 MHz, DMSO-d$_6$) $\delta$ 9.39 (d, $J$ = 2.0 Hz, 1H), 9.36 (d, $J$ = 2.0 Hz, 1H), 9.32 (d, $J$ = 2.0 Hz, 1H), 9.28 (d, $J$ = 2.0 Hz, 1H), 9.06 (s, 1H). NMR shifts agreed with the reported values.[69]

**9-Amino-10-nitro-1,4,5,8-tetraazaphenanthrene.** Sodium methanolate was prepared by dissolving metallic sodium (1.42 g, 62 mmol) in 80 mL of methanol. After reaction of the sodium, hydroxylamine hydrochloride (2.05 g, 29.5 mmol), previously dissolved in 30 mL of methanol, was added. After settling, the salt formed was filtered off and the filtrate was poured onto a suspension of 9-nitro-1,4,5,8-tetraazaphenanthrene (1.00 g, 4.32 mmol) in 35 mL of methanol kept at reflux. The progress of the reaction was monitored by TLC (SiO$_2$, CHCl$_3$/acetone, 8 : 2). After about 2 hours, the reaction was stopped, and the reaction medium cooled down to room temperature. The yellow precipitate was recovered by filtration, rinsed with cold methanol and with diethylether. This reaction yielded 9-amino-10-nitro-1,4,5,8-tetraazaphenanthrene in the form of a yellow powder (1.03 g, 98%). **$^1$H NMR** (300 MHz, DMSO-d$_6$) $\delta$ 9.34 (d, $J$ = 2.1 Hz, 1H), 9.20 (d, $J$ = 2.1 Hz, 1H), 8.94 (d, $J$ = 2.1 Hz, 1H), 8.88 (d, $J$ = 2.1 Hz, 1H), 7.91 (s, 2H). NMR shifts agreed with the reported values.[69]

**9,10-Diamino-1,4,5,8-tetraazaphenanthrene.** Hydrazine hydrate 98% (2.2 mL, 44.9 mmol) in 10 mL of 1 : 1 ethanol/ dioxane is added dropwise to a hot suspension of 9-amino-10-nitro-1,4,5,8-tetraazaphenanthrene (0.85 g, 3.4 mmol) in 130 mL of 1 : 1 ethanol/dioxane, containing 0.7 g Pd/C 10%. The mixture was heated under reflux and monitored by TLC until the starting material disappeared (Al$_2$O$_3$, CHCl$_3$/EtOH 98 : 2). Hot filtration on Celite removed the catalyst, and the appearance of red needles was noted as the medium cooled. The needles were collected by filtration and the filtrate was evaporated to dryness before being triturated in water at room temperature, filtered and washed with water and diethylether. The dark-red powder was then dried under vacuum, yielding 9,10-diamino-1,4,5,8-tetraazaphenanthrene (0.51 g, 71%). **$^1$H NMR** (300 MHz, DMSO-d$_6$) $\delta$ 8.96 (d, $J$ = 2.1 Hz, 2H), 8.88 (d, $J$ = 2.1 Hz, 2H), 5.77 (s, 4H). NMR shifts agreed with the reported values.[69]

**[Os(phen)$_2$(diNH$_2$TAP)]$^{2+}$·2PF$_6^-$ (1).** 1,4,5,8-Tetraazaphenanthrene-9,10-diamine (11.2 mg, 0.053 mmol) and [Os(phen)$_2$Cl$_2$] (30.0 mg, 0.048 mmol) were suspended in ethylene glycol (3 mL) in a microwave tube. The solution was degassed by three vacuum/argon cycles. The mixture was heated for 2 h at 160 °C under microwave irradiation (maximum power = 600 W). After reaction, the mixture was brought to room temperature and a saturate NH$_4$PF$_6$ aqueous solution was added to induce precipitation of the complex.

The precipitate was collected by centrifugation and washed three times with cold water and Et$_2$O. The crude product was then purified by column chromatography (Al$_2$O$_3$, CH$_3$CN/H$_2$O 100 : 0 to 93 : 7) to yield [Os(phen)$_2$(diNH$_2$TAP)]$^{2+}$ as a dark-red powder (23.0 mg, 39%). **$^1$H NMR** (500 MHz, CD$_3$CN) $\delta$ 8.48 (dd, $J$ = 8.3, 1.2 Hz, 2H), 8.43 (dd, $J$ = 8.3, 1.2 Hz, 2H), 8.41 (d, $J$ = 3.0 Hz, 2H), 8.25 (s, 4H), 7.95 (dd, $J$ = 5.4, 1.2 Hz, 2H), 7.88 (dd, $J$ = 5.4, 1.2 Hz, 2H), 7.81 (d, $J$ = 3.0 Hz, 2H), 7.60 (td, $J$ = 8.4, 5.4 Hz, 4H), 5.35 (s, 4H). HRMS(ESI) $m/z$ calculated for [C$_{34}$H$_{24}$N$_{10}$$^{184}$Os]$^{2+}$ = 378.08497; found 378.08524.

**[Os(TAP)$_2$(NO$_2$NH$_2$TAP)]$^{2+}$·2PF$_6^-$ (2).** 9-NH$_2$-10-NO$_2$-1,4,5,8-tetraazaphenanthrene (12.7 mg, 0.0525 mmol) and [Os (TAP)$_2$Cl$_2$] (30.0 mg, 0.048 mmol) were suspended in ethylene glycol (3 mL) in a microwave tube. The solution was degassed by three vacuum/argon cycles. The mixture was heated for 2 h at 160 °C under microwave irradiation (maximum power = 600 W). After reaction, the mixture was brought to room temperature and the complex was precipitated from by the gradual addition of a 3 : 1 Et$_2$O/EtOH mixture. The precipitate was collected by centrifugation and washed three times with Et$_2$O. The crude product was purified by size exclusion chromatography (Sephadex LH-20, conditioned in MeOH). The desired fraction was collected, and the solvent was removed under reduced pressure. The dark solid was dissolved in water and isolated as a PF$_6^-$ salt after ion metathesis. The precipitate was collected by centrifugation and washed three times with cold water and Et$_2$O to yield [Os(TAP)$_2$(NO$_2$NH$_2$TAP)]$^{2+}$ as a dark-brown solid (18.7 mg, 36%). **$^1$H NMR** (500 MHz, CD$_3$CN) $\delta$ 8.94 (d, $J$ = 2.9 Hz, 1H), 8.92 (d, $J$ = 2.9 Hz, 1H), 8.85 (dd, $J$ = 2.9, 1.1 Hz, 2H), 8.73 (d, $J$ = 3.0 Hz, 1H), 8.63 (dt, $J$ = 3.0, 1.6 Hz, 4H), 8.27 (t, $J$ = 2.9 Hz, 2H), 8.20 (d, $J$ = 2.9 Hz, 1H), 8.13 (d, $J$ = 2.9 Hz, 1H), 8.11 (d, $J$ = 2.9 Hz, 1H), 7.81 (d, $J$ = 3.0 Hz, 2H). HRMS(ESI) $m/z$ calculated for [C$_{30}$H$_{18}$O$_2$N$_{14}$$^{184}$Os]$^{2+}$ = 395.06255; found 395.06271.

**[Os(TAP)$_2$(diNH$_2$TAP)]$^{2+}$·2PF$_6^-$ (3).** [Os(TAP)$_2$(diNH$_2$TAP)]$^{2+}$ was obtained using the synthetic procedure described for [Os(TAP)$_2$(NO$_2$NH$_2$TAP)]$^{2+}$ with 1,4,5,8-tetraazaphenanthrene-9,10-diamine (11.2 mg, 0.053 mmol) to yield [Os(TAP)$_2$(diNH$_2$TAP)]$^{2+}$ a dark-brown solid (22.5 mg, 44%). **$^1$H NMR** (500 MHz, CD$_3$CN) $\delta$ 8.83 (dd, $J$ = 9.4, 2.9 Hz, 4H), 8.63 (d, $J$ = 2.9 Hz, 2H), 8.61 (s, 4H), 8.16 (dd, $J$ = 5.7, 2.9 Hz, 4H), 7.84 (d, $J$ = 2.9 Hz, 2H), 5.46 (s, 4H). HRMS(ESI) $m/z$ calculated for [C$_{30}$H$_{20}$N$_{14}$$^{184}$Os]$^{2+}$ = 380.07547; found 380.07557.

**[Ru(phen)$_2$(diiminoTAP)]$^{2+}$·2PF$_6^-$ (4) and [Ru(phen)$_2$ (diNH$_2$TAP)]$^{2+}$·2PF$_6^-$ (5).** [Ru(phen)$_2$Cl$_2$] (300 mg, 0.56 mmol) and 9,10-diamino-1,4,5,8-tetraazaphenanthrene (130 mg, 0.61 mmol) were placed in 20 mL of an argon purged EtOH/ H$_2$O (1 : 1) mixture. The mixture was heated at reflux under argon and protection from ambient light. After 6 h, the reaction was cooled down to room temperature and evaporated to dryness. The residue was purified by column chromatography (Al$_2$O$_3$, CH$_3$CN/H$_2$O 99 : 1 to 90 : 10), yielding [Ru(phen)$_2$ (diNH$_2$TAP)]$^{2+}$ as an orange solid and [Ru(phen)$_2$ (diiminoTAP)]$^{2+}$ as a pink solid. The solids were dissolved in water and isolated as PF$_6^-$ salts after ion metathesis. The precipitates were collected by centrifugation and washed three

times with cold water and $Et_2O$ to yield $[Ru(phen)_2(diNH_2TAP)]^{2+}$ (367 mg, 68%) and $[Ru(phen)_2(diiminoTAP)]^{2+}$ (124 mg, 23%). Characterization for $[Ru(phen)_2(diNH_2TAP)]^{2+}$ matched those previously reported in the literature.[31] **[Ru(phen)_2(diiminoTAP)]^{2+}**, **$^1$H NMR** (300 MHz, $CD_3CN$) $\delta$ 13.39 (s, 2H), 9.10 (d, $J = 2.3$ Hz, 2H), 8.86 (d, $J = 2.3$ Hz, 2H), 8.73 (dd, $J = 8.3, 1.3$ Hz, 2H), 8.63 (dd, $J = 8.3, 1.3$ Hz, 2H), 8.30 (dd, $J = 5.3, 1.3$ Hz, 2H), 8.26 (s, 4H), 7.91 (dd, $J = 5.2, 1.3$ Hz, 2H), 7.83 (dd, $J = 8.3, 5.2$ Hz, 2H), 7.67 (dd, $J = 8.3, 5.2$ Hz, 2H). HRMS(ESI) $m/z$ calculated for $[C_{34}H_{22}N_{10}{}^{96}Ru]^{2+} = 333.05470$; found 333.05504. **[Ru(phen)_2(diNH_2TAP)]^{2+}**, **$^1$H NMR** (300 MHz, $CD_3CN$) $\delta$ 8.73–8.52 (m, 6H), 8.25 (s, 4H), 8.07 (dd, $J = 5.2, 1.3$ Hz, 2H), 7.99 (dd, $J = 5.3, 1.3$ Hz, 2H), 7.81 (d, $J = 2.8$ Hz, 2H), 7.69–7.60 (m, 4H). HRMS(ESI) $m/z$ calculated for $[C_{34}H_{24}N_{10}{}^{96}Ru]^{2+} = 334.06252$; found 334.06296.

**[Ru(TAP)_2(diiminoTAP)]^{2+}·2PF_6$^-$ (6).** $[Ru(TAP)_2Cl_2]$ (300 mg, 0.55 mmol) and 9,10-diamino-1,4,5,8-tetraazaphenanthrene (233 mg, 1.1 mmol) were suspended in 30 mL of water. The mixture was refluxed for 6 h, allowing the solution to adopt a burgundy coloration. After reaction, the mixture was cooled down to room temperature and the solvent removed under reduced pressure. The crude product was purified by column chromatography ($Al_2O_3$, $CH_3CN/H_2O$ 100:0 to 90:10) yielding $[Ru(TAP)_2(diiminoTAP)]^{2+}$ as a pink solid. The solid was dissolved in water and isolated as a $PF_6{}^-$ salt after ion metathesis. The precipitate was collected by centrifugation and washed three times with cold water and $Et_2O$ to yield $[Ru(TAP)_2(diiminoTAP)]^{2+}$ (420 mg, 79%). **$^1$H NMR** (300 MHz, $CD_3CN$) $\delta$ 13.27 (s, 2H), 9.22 (d, $J = 2.7$ Hz, 2H), 9.12 (d, $J = 2.2$ Hz, 2H), 9.01 (d, $J = 2.8$ Hz, 2H), 8.88 (d, $J = 2.3$ Hz, 2H), 8.63 (s, 4H), 8.58 (d, $J = 2.8$ Hz, 2H), 8.21 (d, $J = 2.8$ Hz, 2H). HRMS(ESI) $m/z$ calculated for $[C_{30}H_{18}N_{14}{}^{96}Ru]^{2+} = 335.04519$; found 334.04564.

**[Ru(TAP)_2(NO_2NH_2TAP)]^{2+}·2PF_6$^-$ (7).** $[Ru(TAP)_2Cl_2]$ (200 mg, 0.38 mmol) and 9-$NH_2$-10-$NO_2$-1,4,5,8-tetraazaphenanthrene (110 mg, 0.45 mmol) were suspended in 6 mL of water. The suspension was heated for 1 h at 120 °C under microwave irradiation (maximum power = 200 W). After reaction, the mixture was centrifuged to remove insoluble materials and the filtrate was evaporated under reduced pressure. The residue was purified by column chromatography ($Al_2O_3$, $CH_3CN/H_2O$ 98:2 to 90:10), yielding $[Ru(TAP)_2(NO_2NH_2TAP)]^{2+}$ as an orange solid. The solid was dissolved in water and isolated as a $PF_6{}^-$ salt after ion metathesis. The precipitate was collected by centrifugation and washed three times with cold water and $Et_2O$ to yield $[Ru(TAP)_2(NO_2NH_2TAP)]^{2+}$ (125 mg, 33%). **$^1$H NMR** (300 MHz, $CD_3CN$) $\delta$ 9.06 (dd, $J = 4.6, 2.8$ Hz, 2H), 8.98 (dd, $J = 2.8, 1.9$ Hz, 2H), 8.90 (d, $J = 2.8$ Hz, 1H), 8.77 (d, $J = 2.8$ Hz, 1H), 8.68–8.56 (m, 4H), 8.33 (dd, $J = 3.6, 2.8$ Hz, 2H), 8.27 (d, $J = 2.8$ Hz, 1H), 8.23–8.13 (m, 2H), 7.86 (d, $J = 2.9$ Hz, 1H), 7.76 (s, 2H). HRMS(ESI) $m/z$ calculated for $[C_{30}H_{18}O_2N_{14}{}^{96}Ru]^{2+} = 351.04011$; found 351.04050.

**[Ru(TAP)_2(diNH_2TAP)]^{2+}·2PF_6$^-$ (8).** $[Ru(TAP)_2(9-NH_2-10-NO_2TAP)]^{2+}·2PF_6{}^-$ (100 mg, 0.10 mmol) and 40 mg of Pd/C 10% were suspended in 15 mL of argon purged EtOH/MeOH (1:1) mixture. Hydrazine hydrate (85 µL, 87.5 mg; 1.75 mmol)

was added and the mixture was heated at reflux under argon for 8 h. After reaction, the mixture was brought to room temperature and filtered through a Celite pad to remove the palladium catalyst. The Celite pad was washed with 50 mL of MeOH to recover all the complex. After evaporation of the filtrate, the residue was purified by column chromatography ($Al_2O_3$, $CH_3CN/H_2O$ 95:5 to 85:15) to yield $[Ru(TAP)_2(diNH_2TAP)]^{2+}$ as an orange powder (76 mg, 78%). **$^1$H NMR** (300 MHz, $CD_3CN$) $\delta$ 8.98 (dd, $J = 5.0, 2.8$ Hz, 1H), 8.75 (d, $J = 2.8$ Hz, 1H), 8.62 (s, 1H), 8.22 (dd, $J = 2.8, 1.7$ Hz, 1H), 7.89 (d, $J = 2.8$ Hz, 1H). HRMS(ESI) $m/z$ calculated for $[C_{30}H_{20}N_{14}{}^{96}Ru]^{2+} = 336.05302$; found 334.05341.

## Results and discussion

### Synthesis

The ligands of interest, *i.e.* 1,4,5,8-tetraazaphenanthrene (TAP), 9-amino-10-nitro-1,4,5,8-tetraazaphenanthrene ($NO_2NH_2TAP$) and 9,10-diamino-1,4,5,8-tetraazaphenanthrene ($diNH_2TAP$) were synthesized following a combination of reported procedures but were optimized for larger scale production (~100 g of starting material) (Fig. 1).[68–73] First a condensation of 4-nitro-1,2-diaminobenzene and glyoxal in refluxing ethanol was performed to obtain the corresponding 6-nitroquinoxaline in 80% yield. Vicarious nucleophilic substitution with hydroxylamine using sodium methanolate yielded 5-amino-6-nitroquinoxaline in a 56% yield, which was then reduced using hydrazine hydrate with 10% Pd/C to yield 5,6-diamino-quinoxaline in 98% yield. This derivative was pivotal for the synthesis, as it not only allowed for the desired 1,4,5,8-tetraazaphenanthrene to be obtained in an 80% yield following condensation with glyoxal, but it is also a central fragment for the synthesis of 9-amino-10-nitro-1,4,5,8-tetraazaphenanthrene and 9,10-diamino-1,4,5,8-tetraazaphenanthrene. As such, 5,6-diamino-quinoxaline was protected using *p*-toluenesulfonyl chloride in pyridine. The subsequent nitration was not optimized for large scale synthesis and was therefore carried out several times on 7 grams of starting material (72% of average yield). Deprotection was performed using sulfuric acid and water, leading to the corresponding diamino derivative (96% yield) that was condensed with glyoxal to yield 9-nitro-1,4,5,8-tetraazaphenanthrene in a 52% yield. Amination led to the formation of the 9-amino-10-nitro-1,4,5,8-tetraazaphenanthrene in 98% yield that could be further reduced, using hydrazine hydrate with 10% Pd/C, to form the final product 9,10-diamino-1,4,5,8-tetraazaphenanthrene in 71% yield.

The synthesis of the Os(ɪɪ) photosensitizers was straightforward. $[Os(phen)_2Cl_2]$ and $[Os(TAP)_2Cl_2]$ precursors were prepared according to reported procedures using $(NH_4)_2OsCl_6$ freshly prepared from $OsO_4$. $[Os(phen)_2Cl_2]$ and $[Os(TAP)_2Cl_2]$ were then respectively reacted with 1,4,5,8-tetraazaphenanthrene-9,10-diamine in ethylene glycol at 160 °C under microwave irradiation for 2 hours to yield $[Os(phen)_2(diNH_2TAP)]^{2+}$ (**1**) and $[Os(TAP)_2(diNH_2TAP)]^{2+}$ (**3**) in 39% and 44% isolated

yields, respectively. $[Os(TAP)_2(NO_2NH_2TAP)]^{2+}$ (**2**) was also synthesized in 36% yield for comparison purposes.

The synthesis of $[Ru(phen)_2(diNH_2TAP)]^{2+}$ (**5**) was already reported and was thus performed according to a previously published procedure through the reaction between $[Ru(phen)_2Cl_2]$ and 9,10-diamino-1,4,5,8-tetraazaphenanthrene in EtOH/Water mixtures.[31] Although not reported, this reaction resulted in the formation of two products: $[Ru(phen)_2(diNH_2TAP)]^{2+}$ (**5**) and $[Ru(phen)_2(diiminoTAP)]^{2+}$ (**4**) that could be separated by column chromatography on alumina. $[Ru(phen)_2(diNH_2TAP)]^{2+}$ (**5**) was isolated in 68% yield as an orange solid, whereas $[Ru(phen)_2(diiminoTAP)]^{2+}$ (**4**) was isolated in 23% yield as a pink solid. It should be noted that Ishow *et al.* reported in 1999 that "*Attempts to prepare the precursor diamino complex $[Ru(bpy)_2(diNH_2phen)]^{2+}$ by reaction of 5,6-diamino-1,10-phenanthroline with $[Ru(bpy)_2Cl_2]$ in the presence of $AgCF_3SO_3$ mostly gave the phenanthrolinediimido complex and the dinuclear $[(bpy)_2Ru(tpphz)Ru(bpy)_2]^{4+}$ arising from the auto-condensation of the phendiamine in oxidizing conditions*".[91] Note that similar phenanthrolinediimido complexes have also been reported using different approaches.[92–95] When similar reaction conditions were applied using $[Ru(TAP)_2Cl_2]$ with 9,10-diamino-1,4,5,8-tetraazaphenanthrene in EtOH/Water mixtures or in pure water, the reaction exclusively led to the formation of $[Ru(TAP)_2(diiminoTAP)]^{2+}$ (**6**) with no formation of the desired $[Ru(TAP)_2(diNH_2TAP)]^{2+}$ (**8**). This difference in reactivity is probably a direct consequence of the redox potential of the ruthenium centre (*vide infra*) that is a stronger oxidant when chelated to π-accepting ligands such as 1,4,5,8-tetraazaphenanthrene compared to 1,10-phenanthroline. Hence, an alternative approach proceeding *via* the synthesis of the precursor complex $[Ru(TAP)_2(9-NH_2-10-NO_2-TAP)]^{2+}$ (**7**) was developed. This complex was synthesized from the reaction between [Ru(TAP)_2Cl_2] and 9-NH_2-10-NO_2-1,4,5,8-tetraazaphenanthrene in moderate yields of 33%. This resulted from the very low solubility of 9-NH_2-10-NO_2-1,4,5,8-tetraazaphenanthrene in most

common organic solvents which prevented any efficient reaction, but facilitated the purification procedure. The chemical reduction of $[Ru(TAP)_2(9-NH_2-10-NO_2-TAP)]^{2+}$ (**7**) to the corresponding $[Ru(TAP)_2(diNH_2TAP)]^{2+}$ (**8**) was then investigated. Procedures using hydrazine hydrate and Pd/C, RANEY® Nickel, or $H_2$ on Pd/C have been reported for reduction of nitro groups on ruthenium complexes. Hydrazine hydrate in EtOH/MeOH mixture in combination with Pd/C 10% was found to be optimal to reduce the nitro group of **7** to obtain $[Ru(TAP)_2(diNH_2TAP)]^{2+}$ (**8**) as an orange solid in 78% yield.

### Electrochemistry

All photosensitizers were electrochemically characterized by differential pulse voltammetry and cyclic voltammetry in acetonitrile containing 0.1 M TBAPF_6 and the electrochemical data are tabulated in Table 1. The electrochemical data of $[Os(phen)_2(diNH_2TAP)]^{2+}$ (**1**) showed three reduction peaks at −0.91 V, −1.34 and −1.62 V *vs.* Ag/AgCl. The first peak was attributed to the one-electron reduction of the 1,4,5,8-tetraazaphenanthrene backbone of 1,4,5,8-tetraazaphenanthrene-9,10-diamine. The peak at −1.34 V and −1.62 V *vs.* Ag/AgCl corresponds well to reported reduction potentials of the ancillary 1,10-phenanthroline ligands. Oxidation waves at +0.82 and +1.29 V *vs.* Ag/AgCl were measured. The first peak was attributed to an oxidation of the amine functional group, as this potential is too cathodic to correspond to the Os(II/III) oxidation, which is instead well matched to the +1.29 V *vs.* Ag/AgCl peak. Conversely, with $[Os(TAP)_2(diNH_2TAP)]^{2+}$ (**3**), the first reduction was measured at −0.64 V *vs.* Ag/AgCl and can safely be attributed to the reduction of one of the ancillary 1,4,5,8-tetraazaphenanthrene ligands. Indeed, the reduction of 1,4,5,8-tetraazaphenanthrene-9,10-diamine typically occurs at more negative potentials due to the increased electron density afforded by the two amino groups. An oxidation peak was recorded at +0.88 V *vs.* Ag/AgCl corresponding to the oxidation of the amine, whereas the metal centre oxidation was recorded at +1.74 V *vs.* Ag/AgCl. This value is more positive than typi-

**Table 1** Electrochemical properties of complexes **1–8** and reference complexes in acetonitrile at room temperature

| Complexes | $E_{ox}$ [a] | $E_{red}$ [a] | Ref. |
|---|---|---|---|
| $[Os(phen)_2(diNH_2TAP)]^{2+}$ (**1**) | +0.82; +1.29 | −0.90; −1.34, −1.59 | b |
| $[Os(TAP)_2(NO_2NH_2TAP)]^{2+}$ (**2**) | +1.63 | −0.54; −0.75; −0.99; −1.17; −1.54 | b |
| $[Os(TAP)_2(diNH_2TAP)]^{2+}$ (**3**) | +0.88; +1.74 | −0.64; −0.81; −1.14; −1.51 | b |
| $[Ru(phen)_2(diiminoTAP)]^{2+}$ (**4**) | +1.57 | −0.32; −0.74; −1.54 | b |
| $[Ru(phen)_2(diNH_2TAP)]^{2+}$ (**5**) | +0.82; +1.71 | −0.93; −1.42; −1.65 | b |
| $[Ru(TAP)_2(diiminoTAP)]^{2+}$ (**6**) | +1.84 | −0.12; −0.74; −0.94; −1.08; −1.12 | b |
| $[Ru(TAP)_2(NO_2NH_2TAP)]^{2+}$ (**7**) | > +2 | −0.60; −0.82; −0.99; −1.12 | b |
| $[Ru(TAP)_2(diNH_2TAP)]^{2+}$ (**8**) | +0.88; > +2 | −0.73; −0.89; −1.13 | b |
| | | | |
| $[Ru(phi)_3]^{2+}$ | +1.27; +1.46 | −0.34; −0.56; −0.71; −0.91; −1.07 | 96 |
| $[Ru(bpy)(diiminobenzene)_2]^{2+}$ | +1.24 | −0.39; −0.83; −1.56; −1.92 | 95 |
| $[Ru(bpy)_2(diiminonaphthalene)]^{2+}$ | +1.08 | −0.80; −1.42; −1.94 | 95 |
| $[Ru(bpy)_2(phi)]^{2+}$ | +1.02 | −0.86; −1.48; −1.97 | 95 |
| $[Ru(phen)_3]^{2+}$ | +1.33 | −1.31; −1.48 | 97 |
| $[Ru(TAP)_3]^{2+}$ | +1.98 | −0.71; −0.84; −1.06; −1.56; −1.76 | 98 |

[a] Electrochemical data (in V *vs.* Ag/AgCl) were measured with tetrabutylammonium hexafluorophosphate (0.1 M) as supporting electrolyte with a scan rate of 100 mV s⁻¹. [b] This work.

cally observed with Os(II) complexes, but is in agreement with the electron-withdrawing nature of 1,4,5,8-tetraazaphenanthrene-type ligands. [Os(TAP)$_2$(NO$_2$NH$_2$TAP)]$^{2+}$ (**2**) exhibited a first reduction peak at −0.54 V vs. Ag/AgCl attributed to the reduction of the 9-amino-10-nitro-1,4,5,8-tetraazaphenanthrene ligand. The metal-centred oxidation potential of [Os(TAP)$_2$(NO$_2$NH$_2$TAP)]$^{2+}$ was recorded at +1.63 V vs. Ag/AgCl, in line with the introduction of two electron-withdrawing 1,4,5,8-tetraazaphenanthrene ancillary ligands. The electrochemical data suggested interesting excited-state properties of the Os(II) complexes that could drive several reactions (*vide infra*). Interestingly, none of the electrochemical results for the photosensitizers bearing the 9-amino-10-nitro-1,4,5,8-tetraazaphenanthrene ligand showed a wave that could correspond to the oxidation of the amine group. This likely suggests the role of the nitro group in stabilizing the amine functionality and preventing its oxidation.

The electrochemical data obtained with the Os(II) photosensitizers facilitated the interpretation of the data for the Ru(II) photosensitizers. [Ru(phen)$_2$(diNH$_2$TAP)]$^{2+}$ (**5**) exhibited two oxidation waves centred at +0.82 and +1.71 V vs. Ag/AgCl. The first wave was attributed to the oxidation of the amine functional group, while the second peak was attributed to the Ru(II/III) oxidation. Similar conclusions were drawn for [Ru(TAP)$_2$(diNH$_2$TAP)]$^{2+}$ (**7**) where the first oxidation, centred at +0.88 V vs. Ag/AgCl, was attributed to the oxidation of the amine moiety. However, in this photosensitizer, oxidation of the Ru(II) centre occurred at potentials greater than 2 V vs. Ag/AgCl, in line with other Ru(II) complexes carrying the 1,4,5,8-tetraazaphenantrene ligand such as [Ru(TAP)$_3$]$^{2+}$.[98]

Finally, with [Ru(phen)$_2$(diiminoTAP)]$^{2+}$ (**4**) and [Ru(TAP)$_2$(diiminoTAP)]$^{2+}$ (**6**) the metal-centred oxidations occurred at potentials of +1.57 V and +1.84 V vs. Ag/AgCl, respectively. Comparison of [Ru(phen)$_2$(diiminoTAP)]$^{2+}$ (**4**) with [Ru(phen)$_3$]$^{2+}$ supported the theory that the diimino scaffold decreased the electron density around the metal centre and rendered the Ru(II) harder to oxidize. Compounds bearing an *o*-quinonediimine scaffold have been scarcely reported in the literature, but this observation is in line with these reports.[96] Most representative examples include work by Barton,[96] focusing of [Ru(phi)$_3$]$^{2+}$ (phi = *o*-phenanthrenequinone-diimine) and by Zehnder,[95] who developed three diimino complexes, namely [Ru(bpy)(diiminobenzene)$_2$]$^{2+}$, [Ru(bpy)$_2$(diiminonaphthalene)]$^{2+}$ and [Ru(bpy)$_2$(phi)]$^{2+}$ where the diimino ligands were shown to increase the oxidation potential of the ruthenium complex compared to classical polypyridyl Ru(II) complexes.

Regarding the reduction potentials, from Zehnder's and Barton's work, it is concluded that the addition of diimino ligands shifts the reduction potentials to more positive values. Reduction potentials centred around −0.8 V vs. Ag/AgCl were reported for [Ru(bpy)$_2$(diiminonaphthalene)]$^{2+}$ and [Ru(bpy)$_2$(phi)]$^{2+}$, whereas for [Ru(bpy)(diiminobenzene)$_2$]$^{2+}$ and [Ru(phi)$_3$]$^{2+}$ reduction waves at −0.39 V and −0.34 V vs. Ag/AgCl were reported respectively. Furthermore, a second reduction wave of [Ru(bpy)(diiminobenzene)$_2$]$^{2+}$ was centred at −0.83 V vs. Ag/AgCl, a value too anodic to be attributed to a

reduction of the 2,2′-bipyridine ligand, that was therefore attributed to the reduction of the second diiminobenzene ligand. For complexes bearing only one "diimino-type" ligand, the second reduction has been reported at potentials more negative than −1.56 V vs. Ag/AgCl and have therefore be attributed to reduction of one of the ancillary 2,2′-bipyridine ligands. For [Ru(phi)$_3$]$^{2+}$, six successive reductions were recorded, with the first three being centred at −0.34 V, −0.56 V and −0.71 V vs. Ag/AgCl, respectively, and corresponding to the successive reductions of each "phi" ligand. For [Ru(phen)$_2$(diiminoTAP)]$^{2+}$ (**4**), several reduction waves were recorded at −0.32 V, −0.74 V and −1.54 V vs. Ag/AgCl. Reduction potentials for [Ru(phen)$_3$]$^{2+}$ indicated that the first reduction centred on 1,10-phenanthroline only occurs at potentials more negative than −1.31 V vs. Ag/AgCl. Therefore, the first and second reductions of complex **4** were attributed to the reduction of the diiminoTAP ligand and the third reduction wave attributed to an ancillary 1,10-phenanthroline reduction. Regarding [Ru(TAP)$_2$(diiminoTAP)]$^{2+}$ (**6**), reduction events at −0.12, −0.74, −0.94, −1.08 and −1.12 V vs. Ag/AgCl were obtained. By comparison with the parent compound [Ru(TAP)$_3$]$^{2+}$, the first reduction wave was attributed to a reduction of the diiminoTAP ligand, whereas subsequent reduction events could not be unambiguously attributed. Notably, the first reduction wave for [Ru(TAP)$_2$(diiminoTAP)]$^{2+}$ (**6**) was exceptionally positive compared to other classical complexes, an observation that probably resulted from the ancillary 1,4,5,8-tetraazaphenanthrene ligands that, due to their highly π-accepting character, drained the ruthenium centre of its electron density. As a result, more electron density was donated from the diiminoTAP ligand, making it easier to reduce than in [Ru(phen)$_2$(diiminoTAP)]$^{2+}$ (**4**), where the 1,10-phenanthroline ligands are less π-accepting.

### Photophysical properties and theoretical calculations

The ground-state properties of the eight photosensitizers were first characterized by UV-Visible absorption measurements in acetonitrile (Fig. 2). Most of the photosensitizers exhibited absorption features that are typical for these classes of compounds. Indeed, the three osmium complexes absorbed intensely in the visible range with molar absorption coefficients in the 16 100–21 300 M$^{-1}$ cm$^{-1}$ range between 456 and 484 nm. [Ru(phen)$_2$(diNH$_2$TAP)]$^{2+}$ (**5**) and [Ru(TAP)$_2$(diNH$_2$TAP)]$^{2+}$ (**7**) also exhibited classical features, namely absorption bands in the UV region attributed to ligand centred (LC) transitions and a broad absorption band between 400 nm and 480 nm attributed to metal-to-ligand charge transfer (MLCT) transitions. The molar absorption coefficients were in the 14 700–17 600 M$^{-1}$ cm$^{-1}$ range between 437 and 467 nm. Interestingly, in [Ru(phen)$_2$(diiminoTAP)]$^{2+}$ (**4**) and [Ru(TAP)$_2$(diiminoTAP)]$^{2+}$ (**6**), the visible absorption features were red-shifted to 535 nm and 520 nm with molar absorption coefficients of 19 700 M$^{-1}$ cm$^{-1}$ and 25 300 M$^{-1}$ cm$^{-1}$, respectively.

Time-dependent density functional theory (TD-DFT) calculations agreed with the classical depiction of metal-to-ligand charge transfer bands for [Ru(phen)$_2$(diNH$_2$TAP)]$^{2+}$ (**5**) and
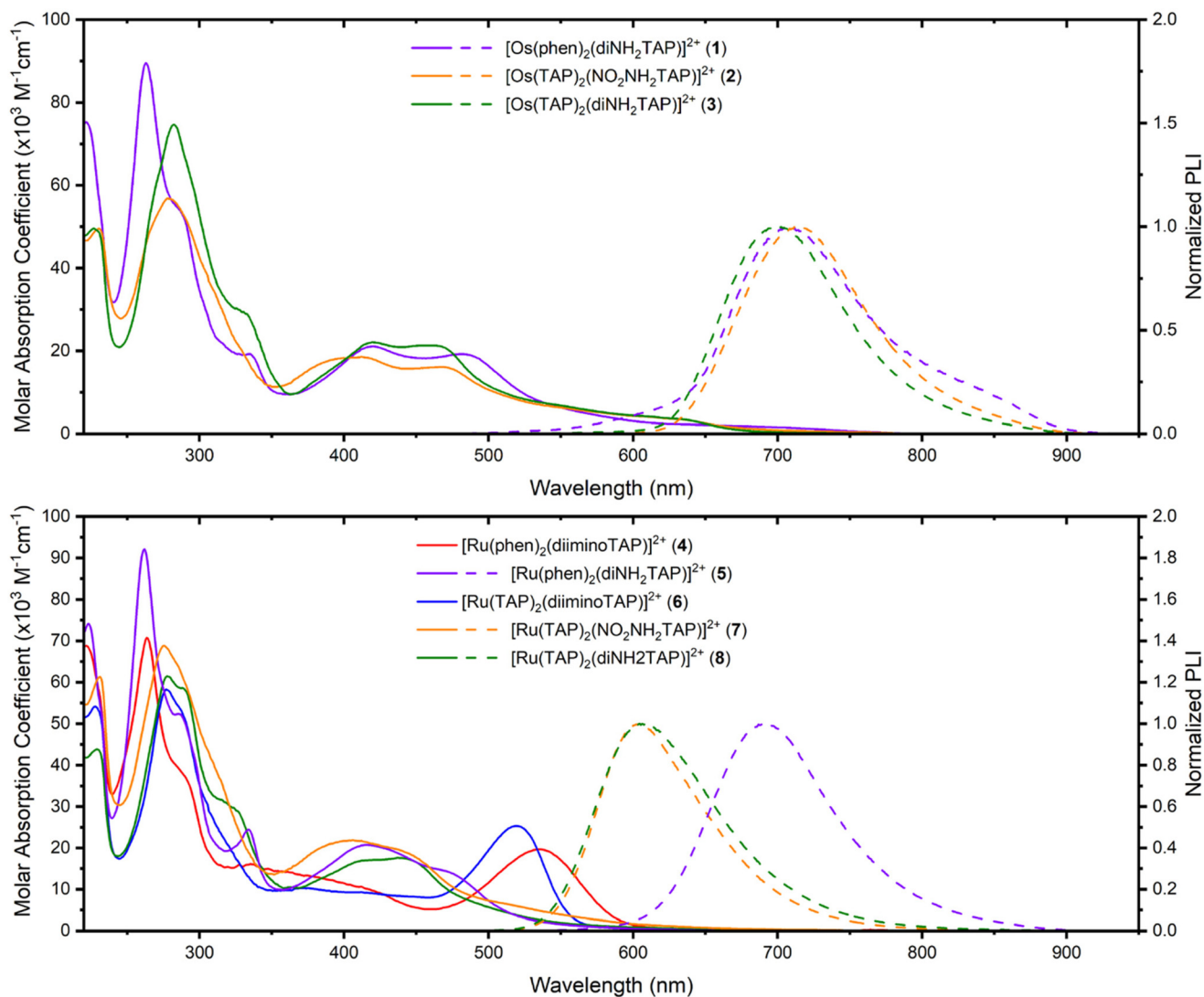
**Fig. 2** Absorption (solid) and photoluminescence (dashed) spectra of Os(II) (top) and Ru(II) (bottom) photosensitizers recorded in acetonitrile at room temperature under argon.

$[Ru(TAP)_2(diNH_2TAP)]^{2+}$ (**7**) where electron density is transferred from the metal centre to the most electron accepting ligand(s) (Fig. 3a and b). For $[Ru(phen)_2(diNH_2TAP)]^{2+}$ (**5**), the transition with the highest probability in the visible range appeared at 409 and 418 nm and involved an electronic transition from the Ru(II) centre to the ancillary ligands. For $[Ru(TAP)_2(diNH_2TAP)]^{2+}$ (**7**), the excitation at 403 nm was consistent with a transition transferring electron density from Ru(II) to the ancillary 1,4,5,8-tetraazaphenanthrene ligands whereas the one at 416 nm additionally transferred electron density on the 9,10-diamino-1,4,5,8-tetraazaphenanthrene ligand. For $[Ru(phen)_2(diiminoTAP)]^{2+}$ (**4**) and $[Ru(TAP)_2(diiminoTAP)]^{2+}$ (**6**) the most probable excitation in the visible part of the spectrum seems to heavily involve the *o*-quinonediimine ligand which could warrant a mixed metal–ligand-to-ligand charge transfer complex, similar to what is observed in prototypical Ir(III) photosensitizers.[99]

The excited-state properties of the photosensitizers were then investigated by steady-state and time-resolved spectroscopic techniques in argon-purged and air-equilibrated acetonitrile. Visible light excitation of all Os(II) photosensitizers led to appreciable photoluminescence centred between 709 and 718 nm. Photoluminescence decay of these excited states was well described by first-order kinetics from which excited-state lifetimes that spanned 228–340 ns under argon were determined. The photoluminescence quantum yields for these Os(II) photosensitizers were unsurprisingly small (Table 2), as expected based on the energy gap law,[100] as well as by the introduction of amine groups that favour non-radiative decay by increasing interactions with the solvent. The exception was $[Os(TAP)_2(NO_2NH_2TAP)]^{2+}$ (**2**) that exhibited an appreciable photoluminescence quantum yield of 0.023 under argon. Considering the electrochemical data gathered for this complex, it is probable that this originates from a stabilization
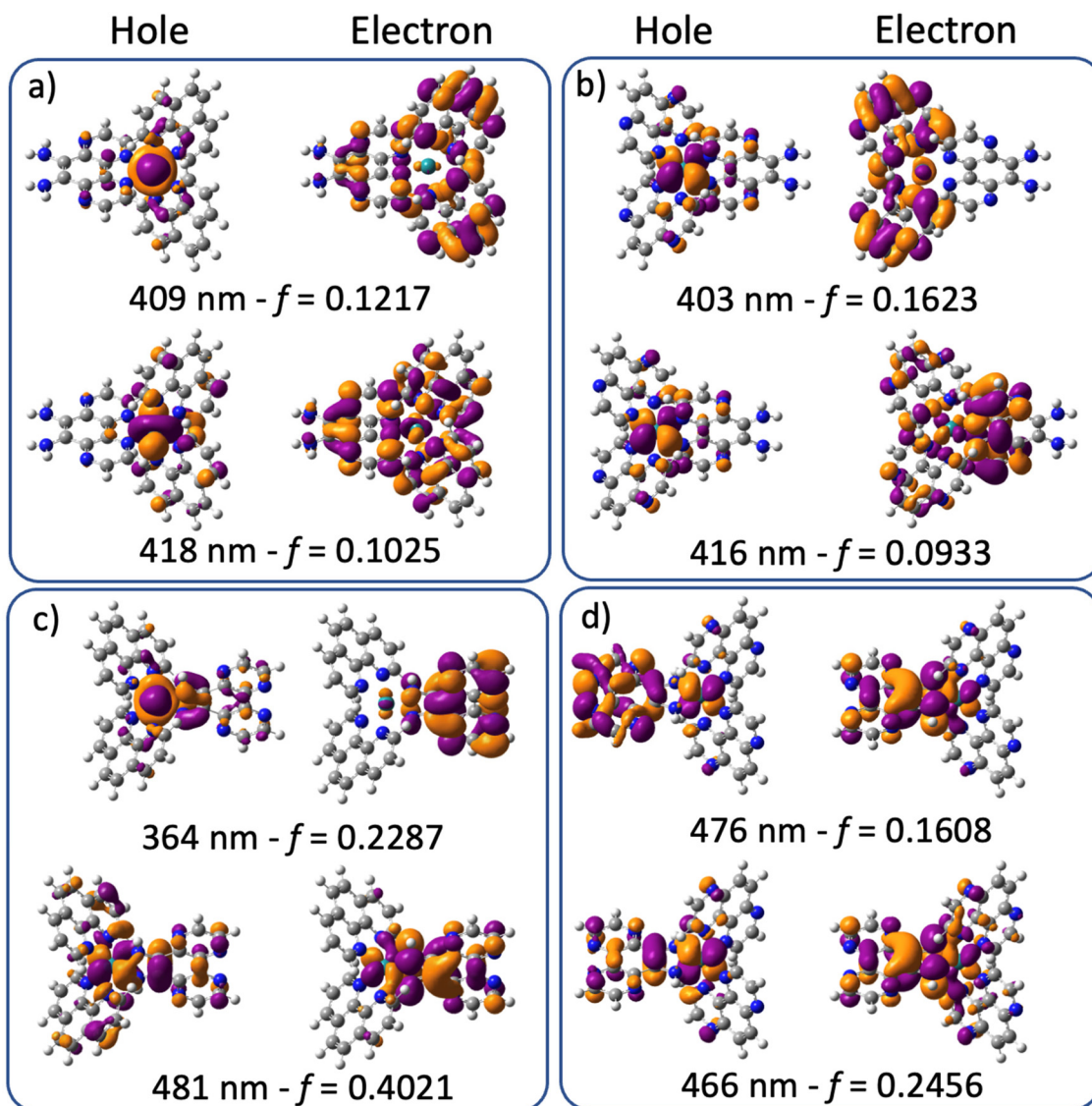
**Fig. 3** Natural Transition Orbitals (NTOs) for [Ru(phen)$_2$(diNH$_2$TAP)]$^{2+}$ (a), [Ru(TAP)$_2$(diNH$_2$TAP)]$^{2+}$ (b), [Ru(phen)$_2$(diiminoTAP)]$^{2+}$ (c) and [Ru(TAP)$_2$(diiminoTAP)]$^{2+}$ (d) involved in each excited state according to the TD-DFT calculations. For each excited state, absorption wavelengths (in nm) and calculated oscillator strengths (f) are listed. See ESI† for additional details on the theoretical calculations.

**Table 2** Photophysical properties of photosensitizers **1–9** in acetonitrile

| Complexes | $\lambda_{Abs}$ (nm), ($\varepsilon$, $10^3$ M$^{-1}$ cm$^{-1}$) | $\lambda_{em}{}^a$ (nm) | $\Phi_{PL}{}^c$ air | $\Phi_{PL}{}^c$ argon | $\tau$ (ns) |
|---|---|---|---|---|---|
| [Os(phen)$_2$(diNH$_2$TAP)]$^{2+}$(**1**) | 263 (89.4), 419 (21.0), 484(19.1) | 717 | 0.00008 | 0.00018 | 67$^b$, 228$^a$ |
| [Os(TAP)$_2$(NO$_2$NH$_2$TAP)]$^{2+}$(**2**) | 279 (56.7), 411 (18.4), 467 (16.1) | 718 | 0.01801 | 0.02283 | 217$^b$, 280$^a$ |
| [Os(TAP)$_2$(diNH$_2$TAP)]$^{2+}$(**3**) | 282 (74.7), 420 (22.1),456 (21.3) | 709 | 0.00128 | 0.00174 | 238$^b$, 340$^a$ |
| [Ru(phen)$_2$(diiminoTAP)]$^{2+}$(**4**) | 263 (70.7), 535 (19.7) | — | — | — | — |
| [Ru(phen)$_2$(diNH$_2$TAP)]$^{2+}$(**5**) | 261 (92.1), 416 (20.7), 467 (14.7) | 699 | 0.00271 | 0.00560 | 292$^b$, 644$^a$ |
| [Ru(TAP)$_2$(diiminoTAP)]$^{2+}$(**6**) | 277 (58.2), 520 (25.3) | — | — | — | — |
| [Ru(TAP)$_2$(NO$_2$NH$_2$TAP)]$^{2+}$(7) | 268 (68.8), 405 (21.8) | 612 | 0.00949 | 0.01125 | 220$^b$, 250$^a$ |
| [Ru(TAP)$_2$(diNH$_2$TAP)]$^{2+}$(**8**) | 278 (61.4), 412 (17.0), 439 (17.6) | 623 | 0.00172 | 0.00205 | 158$^b$, 245$^a$ |

$^a$ Recorded in argon purged acetonitrile. $^b$ Recorded in air equilibrated acetonitrile. $^c$ Measured vs. [Ru(bpy)$_3$]$^{2+}$ ($\Phi_{ref}$ = 0.018 in air equilibrated acetonitrile).

of the amino group by the vicinal nitro group through hydrogen bonding, thus decreasing interactions with the solvent.

$[Ru(phen)_2(diNH_2TAP)]^{2+}$ (**5**), $[Ru(TAP)_2(diNH_2TAP)]^{2+}$ (**7**) and $[Ru(TAP)_2(NO_2NH_2TAP)]^{2+}$ (**8**) were luminescent in acetonitrile with steady-state photoluminescence maxima centred at 699, 623 and 612 nm, respectively. This agrees with an excited state localized on the 9,10-diamino-1,4,5,8-tetraazaphenanthrene ligand for $[Ru(phen)_2(diNH_2TAP)]^{2+}$ (**5**). In contrast, the higher energy luminescence indicated excited-state localization on the ancillary 1,4,5,8-tetraazaphenanthrenes, which is consistent with literature for $[Ru(TAP)_2(diNH_2TAP)]^{2+}$ (**7**) and $[Ru(TAP)_2(NO_2NH_2TAP)]^{2+}$ (**8**). Both Ru(II) photosensitizers bearing *o*-quinonediimine moieties, *i.e.* $[Ru(phen)_2(diiminoTAP)]^{2+}$ (**4**) and $[Ru(TAP)_2(diiminoTAP)]^{2+}$ (**6**), were non-luminescent between 600 and 900 nm. Such behaviour is consistent with a small energy gap between the LUMO and the HOMO that may favour fast non-radiative decay through strong inter-state coupling.

### Excited-state reactivity

The ground-state electrochemical data and the steady-state photoluminescence spectra allowed to determine the corresponding excited-state reduction $(E^*_{red})$ and oxidation $(E^*_{ox})$ potentials in acetonitrile (Table 3).

The photosensitizers exhibited excited-state reduction potentials that are between 1.05 and 1.67 V *vs.* Ag/AgCl (1.24 and 1.86 V *vs.* NHE). $[Ru(TAP)_2(diNH_2TAP)]^{2+}$ (**8**) and $[Ru(TAP)_2(NO_2NH_2TAP)]^{2+}$ (**7**) presented the most positive excited-state reduction potentials, 1.55 and 1.67 V *vs.* Ag/AgCl (1.75 and 1.86 V *vs.* NHE), respectively. Given these excited-state reduction potentials and their large use in the field of photodynamic therapy, we decided to investigate the bimolecular reactivity of these photosensitizers with a prototypical biological substrate, *i.e.* guanosine-5′-monophosphate (GMP). Excited-state quenching experiments were performed in argon purged Tris-HCl aqueous buffer at pH 7.4 with all emissive photosensitizers and GMP. A representative example for the excited-state quenching of $[Os(TAP)_2(NO_2NH_2TAP)]^{2+}$ with GMP is presented in Fig. 4. Overall, appreciable excited-state quenching was only observed for Ru(II) and Os(II) photosensitizers bearing ancillary 1,4,5,8-tetraazaphenanthrene ligands. The quenching rate constants were close to the diffusion limit and were determined for $[Os(TAP)_2(NO_2NH_2TAP)]^{2+}$ and $[Os(TAP)_2(diNH_2TAP)]^{2+}$ as $k_q = 8.9 \times 10^8$ $M^{-1}$ $s^{-1}$ and $6.1 \times 10^8$ $M^{-1}$ $s^{-1}$, respectively. For the corresponding Ru(II) photosensitizers, meanwhile, the quenching rate constants were deter-



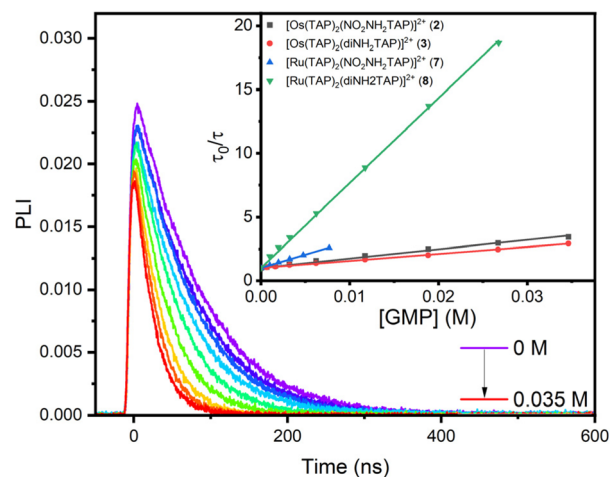**Fig. 4** Time-resolved excited-state quenching of [Os(TAP)$_2$(NO$_2$NH$_2$TAP)]$^{2+}$ and the corresponding Stern–Volmer plots of all photosensitizers undergoing excited-state quenching (inset). Experiments were performed in air-equilibrated Tris HCl buffer (50 mM, pH = 7.4) at room temperature using 440 nm light excitation.

mined to be slightly larger with $k_q = 1.7 \times 10^9$ $M^{-1}$ $s^{-1}$ and $1.3 \times 10^9$ $M^{-1}$ $s^{-1}$ for $[Ru(TAP)_2(diNH_2TAP)]^{2+}$ and $[Ru(TAP)_2(NO_2NH_2TAP)]^{2+}$, respectively. These quenching rate constants agree with the favourable driving force for GMP oxidation by these four photosensitizers in aqueous conditions.

Finally, we sought to investigate whether the excited-state quenching proceeded *via* electron transfer. Using transient absorption spectroscopy, changes in absorption of $[Ru(TAP)_2(diNH_2TAP)]^{2+}$ and $[Ru(TAP)_2(NO_2NH_2TAP)]^{2+}$ using sodium ascorbate as electron donor were initially determined (Fig. 5). In both cases, pulsed light excitation led to absorption changes with a novel transition appearing between 490 and 500 nm that was assigned to the formation of the monoreduced ruthenium photosensitizer. When similar experiments were carried out in the presence GMP in Tris HCl buffer at pH 7.4, the nanosecond transient absorption changes were similar to those obtained with sodium ascorbate, thus confirming excited-state electron transfer from GMP to the ruthenium photosensitizers. While the transient absorption spectra with $[Ru(TAP)_2(NO_2NH_2TAP)]^{2+}$ and GMP matched well with those obtained with sodium ascorbate, the one of obtained with $[Ru(TAP)_2(diNH_2TAP)]^{2+}$ and GMP presented an additional signal at 600 nm that we are currently unable to assign. Unfortunately, such electron transfer products were not

**Table 3** Excited-state reduction and oxidation potential of the emissive photosensitizers

| Complexes | $E^*_{red}$(V *vs.* Ag/AgCl) | $E^*_{ox}$(V *vs.* Ag/AgCl) | $E_{00}$ (eV) |
|---|---|---|---|
| $[Os(phen)_2(diNH_2TAP)]^{2+}$(**1**) | 1.05 | −0.66 | 1.95 |
| $[Os(TAP)_2(NO_2NH_2TAP)]^{2+}$(**2**) | 1.41 | −0.32 | 1.95 |
| $[Os(TAP)_2(diNH_2TAP)]^{2+}$(**3**) | 1.33 | −0.23 | 1.97 |
| $[Ru(phen)_2(diNH_2TAP)]^{2+}$(**5**) | 1.10 | −0.33 | 2.03 |
| $[Ru(TAP)_2(NO_2NH_2TAP)]^{2+}$(**7**) | 1.67 | >−0.27 | 2.27 |
| $[Ru(TAP)_2(diNH_2TAP)]^{2+}$(**8**) | 1.55 | >−0.28 | 2.28 |

**Fig. 5** Transient absorption spectra or $[Ru(TAP)_2(diNH_2TAP)]^{2+}$ and $[Ru(TAP)_2(NO_2NH_2TAP)]^{2+}$ recorded in the presence of 20 mM of sodium ascorbate or with 10 mM of GMP. Spectra were recorded in argon purged Tris-HCl buffer (50, mM, pH = 7.4) 1 μs after le laser pulse and integrated for 50 ns. Samples were excited at 440 nm with a laser fluence of 10 mJ per pulse.

observed with the osmium photosensitizers, preventing a confirmation that excited-state electron transfer from GMP occurred. It is however highly probable, given the similar quenching rate constants and excited-state redox potentials, that excited-state electron transfer is the operative quenching pathway but the associated cage-escape yields are probably lower, as already reported for Os(II) photosensitizers.[101,102]

## Conclusions

The synthesis of eight photosensitizers with Os(II) and Ru(II) metal centres and polyazaaromatic ancillary ligands is reported. All photosensitizers carry one ligand with a 1,4,5,8-tetraazaphenanthrene backbone bearing one ($NO_2NH_2TAP$) or two ($diNH_2TAP$) amine functions. The isolated complexes represent a series of photosensitizers that can also serve as precursors for the development of bridged compounds, useful for solar fuel production or photodynamic therapy and bioimaging applications. For the Ru(II) photosensitizers, a particular chelating behaviour was observed. Indeed, when 1,10-phenanthroline ancillary ligands were used, the reaction between $[Ru(phen)_2Cl_2]$ and 9,10-diamino-1,4,5,8-tetraazaphenanthrene led to the formation of $[Ru(phen)_2(diNH_2TAP)]^{2+}$ (**5**) as the major product and $[Ru(phen)_2(diiminoTAP)]^{2+}$ (**4**) as minor product. However the reaction only yielded $[Ru(TAP)_2(diiminoTAP)]^{2+}$ (**6**) when $[Ru(TAP)_2Cl_2]$ was used as precursor. This difference in reactivity is probably a direct consequence of the redox potential of the ruthenium centre that is a stronger oxidant when chelated to π-accepting ligands such as 1,4,5,8-tetraazaphenanthrene compared to 1,10-phenanthroline. This hypothesis was strengthened by the results of the

reactions with Os(II) complexes, where the *o*-quinonediimine complexes were not obtained under similar conditions. Hence, for Ru(II) complexes, to obtain $[Ru(TAP)_2(diNH_2TAP)]^{2+}$, a synthetic methodology involving the ligand 9-$NH_2$-10-$NO_2$-1,4,5,8-tetraazaphenanthrene was developed. This led to a precursor complex bearing one amino and one nitro group that could be further reduced using hydrazine hydrate on Pd/C with high reaction yields to yield the desired complex.

The coordination pattern was shown to strongly impact the redox properties, as well as the optical properties. Whereas complexes bearing unchelated amine functional groups were almost all luminescent with typical excited-state lifetimes, photosensitizers bearing *o*-quinonediimine scaffolds were non-luminescent in acetonitrile with very short excited-state lifetimes, *i.e.* below the instrument response of our transient absorption spectroscopy apparatus (~2 ns). The short excited-state lifetimes, unusual redox properties and red-shifted absorbance all pointed towards a decreased energy gap between the HOMO and LUMO levels, with strongly coupled excited and ground states, allowing for fast non-radiative decay.

Finally, the luminescent photosensitizers were investigated for their potential use in photodynamic therapy as Type I photosensitizers. Time-resolved quenching experiments and nanosecond transient absorption spectroscopy confirmed that these photosensitizers were competent for excited-state electron transfer, as clearly observed for both $[Ru(TAP)_2(diNH_2TAP)]^{2+}$ and $[Ru(TAP)_2(NO_2NH_2TAP)]^{2+}$. Hence, these novel photosensitizers could find applications as potential photodrugs in photodynamic therapy or as building blocks for larger complexes with π-extended ligands or dyads for bioimaging applications or solar fuels formation.

## Author contributions

The manuscript was written through contributions of all authors. All authors have given approval to the final version of the manuscript.

## Conflicts of interest

There are no conflicts to declare.

## Acknowledgements

# References

1 A. Y. Chan, I. B. Perry, N. B. Bissonnette, B. F. Buksh, G. A. Edwards, L. I. Frye, O. L. Garry, M. N. Lavagnino, B. X. Li, Y. Liang, E. Mao, A. Millet, J. V. Oakley, N. L. Reed, H. A. Sakai, C. P. Seath and D. W. C. MacMillan, *Chem. Rev.*, 2022, **122**, 1485–1542.

2 N. E. S. Tay, D. Lehnherr and T. Rovis, *Chem. Rev.*, 2022, **122**, 2487–2649.

3 M. H. Shaw, J. Twilton and D. W. C. MacMillan, *J. Org. Chem.*, 2016, **81**, 6898–6926.

4 S. A. Archer, A. Raza, F. Dröge, C. Robertson, A. J. Auty, D. Chekulaev, J. A. Weinstein, T. Keane, A. J. H. M. Meijer, J. W. Haycock, S. MacNeil and J. A. Thomas, *Chem. Sci.*, 2019, **10**, 3502–3513.

5 M. R. Gill and J. A. Thomas, *Chem. Soc. Rev.*, 2012, **41**, 3179–3192.

6 A. Raza, S. A. Archer, S. D. Fairbanks, K. L. Smitten, S. W. Botchway, J. A. Thomas, S. MacNeil and J. W. Haycock, *J. Am. Chem. Soc.*, 2020, **142**, 4639–4647.

7 M. Gillard, H. Bonnet, R. Lartia, H. Yacoub, J. Dejeu, E. Defrancq and B. Elias, *Bioconjugate Chem.*, 2023, **34**, 414–421.

8 M. Gillard, G. Piraux, M. Daenen, M. Abraham, L. Troian-Gautier, L. Bar, H. Bonnet, F. Loiseau, H. Jamet, J. Dejeu, E. Defrancq and B. Elias, *Chem. – Eur. J.*, 2022, **28**, e202202251.

9 M. Gillard, L. Troian-Gautier, A. Decottignies and B. Elias, *J. Med. Chem.*, 2024, **67**, 2549–2558.

10 H. Huang, B. Yu, P. Zhang, J. Huang, Y. Chen, G. Gasser, L. Ji and H. Chao, *Angew. Chem., Int. Ed.*, 2015, **54**, 14049–14052.

11 A. Mani, T. Feng, A. Gandioso, R. Vinck, A. Notaro, L. Gourdon, P. Burckel, B. Saubaméa, O. Blacque, K. Cariou, J.-E. Belgaied, H. Chao and G. Gasser, *Angew. Chem., Int. Ed.*, 2023, **62**, e202218347.

12 M. D. Pozza, P. Mesdom, A. Abdullrahman, T. D. Prieto Otoya, P. Arnoux, C. Frochot, G. Niogret, B. Saubaméa, P. Burckel, J. P. Hall, M. Hollenstein, C. J. Cardin and G. Gasser, *Inorg. Chem.*, 2023, **62**, 18510–18523.

13 E. S. Andreiadis, M. Chavarot-Kerlidou, M. Fontecave and V. Artero, *Photochem. Photobiol.*, 2011, **87**, 946–964.

14 M. K. Brennaman, R. J. Dillon, L. Alibabaei, M. K. Gish, C. J. Dares, D. L. Ashford, R. L. House, G. J. Meyer, J. M. Papanikolas and T. J. Meyer, *J. Am. Chem. Soc.*, 2016, **138**, 13085–13102.

15 B. Shan, S. Vanka, T.-T. Li, L. Troian-Gautier, M. K. Brennaman, Z. Mi and T. J. Meyer, *Nat. Energy*, 2019, **4**, 290–299.

16 L. Alibabaei, M. K. Brennaman, M. R. Norris, B. Kalanyan, W. Song, M. D. Losego, J. J. Concepcion, R. A. Binstead, G. N. Parsons and T. J. Meyer, *Proc. Natl. Acad. Sci. U. S. A.*, 2013, **110**, 20008–20013.

17 R. N. Sampaio, L. Troian-Gautier and G. J. Meyer, *Angew. Chem.*, 2018, **130**, 15616–15620.

18 D. Wang, R. N. Sampaio, L. Troian-Gautier, S. L. Marquard, B. H. Farnum, B. D. Sherman, M. V. Sheridan, C. J. Dares, G. J. Meyer and T. J. Meyer, *J. Am. Chem. Soc.*, 2019, **141**, 7926–7933.

19 K. Hu, R. N. Sampaio, J. Schneider, L. Troian-Gautier and G. J. Meyer, *J. Am. Chem. Soc.*, 2020, **142**, 16099–16116.

20 L. H. M. de Groot, A. Ilic, J. Schwarz and K. Wärnmark, *J. Am. Chem. Soc.*, 2023, **145**, 9369–9388.

21 F. Glaser, A. Aydogan, B. Elias and L. Troian-Gautier, *Coord. Chem. Rev.*, 2024, **500**, 215522.

22 N. Sinha, C. Wegeberg, D. Häussinger, A. Prescimone and O. S. Wenger, *Nat. Chem.*, 2023, **15**, 1730–1736.

23 N. Sinha and O. S. Wenger, *J. Am. Chem. Soc.*, 2023, **145**, 4903–4920.

24 D. W. Thompson, A. Ito and T. J. Meyer, *Pure Appl. Chem.*, 2013, **85**, 1257–1305.

25 P. Dongare, B. D. B. Myron, L. Wang, D. W. Thompson and T. J. Meyer, *Coord. Chem. Rev.*, 2017, **345**, 86–107.

26 L. Troian-Gautier and C. Moucheron, *Molecules*, 2014, **19**, 5028–5087.

27 L. Troian-Gautier, L. Marcelis, J. De Winter, P. Gerbaux and C. Moucheron, *Dalton Trans.*, 2017, **46**, 15287–15300.

28 S. De Kreijger, B. Elias and L. Troian-Gautier, *Inorg. Chem.*, 2023, **62**, 16196–16202.

29 J. Bolger, A. Gourdon, E. Ishow and J.-P. Launay, *Inorg. Chem.*, 1996, **35**, 2937–2944.

30 K. Servaty, C. Moucheron and A. Kirsch-De Mesmaeker, *Dalton Trans.*, 2011, **40**, 11704–11711.

31 A. Boisdenghien, C. Moucheron and A. Kirsch-De Mesmaeker, *Inorg. Chem.*, 2005, **44**, 7678–7685.

32 J. Leveque, B. Elias, C. Moucheron and A. Kirsch-De Mesmaeker, *Inorg. Chem.*, 2005, **44**, 393–400.

33 B. Elias, L. Herman, C. Moucheron and A. Kirsch-De Mesmaeker, *Inorg. Chem.*, 2007, **46**, 4979–4988.

34 J. Tisaun, B. Laramée-Milette, J. S. Beckwith, J. Bierwagen, G. S. Hanan, C. Reber, A. Hauser and C. Moucheron, *Inorg. Chem.*, 2021, **60**, 3677–3689.

35 M. G. Pfeffer, C. Müller, E. T. E. Kastl, A. K. Mengele, B. Bagemihl, S. S. Fauth, J. Habermehl, L. Petermann, M. Wächtler, M. Schulz, D. Chartrand, F. Laverdière, P. Seeber, S. Kupfer, S. Gräfe, G. S. Hanan, J. G. Vos, B. Dietzek-Ivanšić and S. Rau, *Nat. Chem.*, 2022, **14**, 500–506.

36 S. Klingler, B. Bagemihl, A. K. Mengele, S. Kaufhold, P. Myllyperkiö, J. Ahokas, M. Pettersson, S. Rau and B. Mizaikoff, *Angew. Chem., Int. Ed.*, 2023, **62**, e202306287.

37 E. S. Ryland, X. Liu, G. Kumar, S. L. Raj, Z.-L. Xie, A. K. Mengele, S. S. Fauth, K. Siewerth, B. Dietzek-Ivanšić, S. Rau, K. L. Mulfort, X. Li and A. A. Cordones, *J. Chem. Phys.*, 2024, **160**, 084307.

38 S. De Kreijger, O. Schott, L. Troian-Gautier, E. Cauët, G. S. Hanan and B. Elias, *Inorg. Chem.*, 2022, **61**, 5245–5254.

39 L. Holden, K. S. Gkika, C. S. Burke, C. Long and T. E. Keyes, *Inorg. Chem.*, 2023, **62**, 2213–2227.

40 C. Moucheron, A. Kirsch-De Mesmaeker and S. Choua, *Inorg. Chem.*, 1997, **36**, 584–592.

41 C. Moucheron and A. Kirsch-De Mesmaeker, *J. Phys. Org. Chem.*, 1998, **11**, 577–583.

42 W. Vanderlinden, M. Blunt, C. C. David, C. Moucheron, A. Kirsch-De Mesmaeker and S. De Feyter, *J. Am. Chem. Soc.*, 2012, **134**, 10214–10221.

43 F. E. Poynton, S. A. Bright, S. Blasco, D. C. Williams, J. M. Kelly and T. Gunnlaugsson, *Chem. Soc. Rev.*, 2017, **46**, 7706–7756.

44 G. Denti, S. Campagna, L. Sabatino, S. Serroni, M. Ciano and V. Balzani, *Inorg. Chem.*, 1990, **29**, 4750–4758.

45 S. Serroni, A. Juris, S. Campagna, M. Venturi, G. Denti and V. Balzani, *J. Am. Chem. Soc.*, 1994, **116**, 9086–9091.

46 S. Campagna, G. Denti, S. Serroni, M. Ciano, A. Juris and V. Balzani, *Inorg. Chem.*, 1992, **31**, 2982–2984.

47 V. Balzani, A. Juris, M. Venturi, S. Campagna and S. Serroni, *Chem. Rev.*, 1996, **96**, 759–834.

48 C. Chiorboli, M. A. J. Rodgers and F. Scandola, *J. Am. Chem. Soc.*, 2003, **125**, 483–491.

49 C. Chiorboli, C. A. Bignozzi, F. Scandola, E. Ishow, A. Gourdon and J.-P. Launay, *Inorg. Chem.*, 1999, **38**, 2402–2410.

50 C. Chiorboli, S. Fracasso, M. Ravaglia, F. Scandola, S. Campagna, K. L. Wouters, R. Konduri and F. M. MacDonnell, *Inorg. Chem.*, 2005, **44**, 8368–8378.

51 S. Campagna, S. Serroni, S. Bodige and F. M. MacDonnell, *Inorg. Chem.*, 1999, **38**, 692–701.

52 L. Troian-Gautier, E. Mugeniwabagara, L. Fusaro, E. Cauët, A. Kirsch-De Mesmaeker and M. Luhmer, *J. Am. Chem. Soc.*, 2017, **139**, 14909–14912.

53 L. Troian-Gautier, E. Mugeniwabagara, L. Fusaro, C. Moucheron, A. Kirsch-De Mesmaeker and M. Luhmer, *Inorg. Chem.*, 2017, **56**, 1794–1803.

54 J. P. Hall, F. E. Poynton, P. M. Keane, S. P. Gurung, J. A. Brazier, D. J. Cardin, G. Winter, T. Gunnlaugsson, I. V. Sazanovich, M. Towrie, C. J. Cardin, J. M. Kelly and S. J. Quinn, *Nat. Chem.*, 2015, **7**, 961–967.

55 P. M. Keane, F. E. Poynton, J. P. Hall, I. V. Sazanovich, M. Towrie, T. Gunnlaugsson, S. J. Quinn, C. J. Cardin and J. M. Kelly, *Angew. Chem., Int. Ed.*, 2015, **54**, 8364–8368.

56 P. M. Keane, K. O'Sullivan, F. E. Poynton, B. C. Poulsen, I. V. Sazanovich, M. Towrie, C. J. Cardin, X.-Z. Sun, M. W. George, T. Gunnlaugsson, S. J. Quinn and J. M. Kelly, *Chem. Sci.*, 2020, **11**, 8600–8609.

57 S. Content and A. Kirsch-De Mesmaeker, *J. Chem. Soc., Faraday Trans.*, 1997, **93**, 1089–1094.

58 C. Moucheron, A. Kirsch-De Mesmaeker and J. M. Kelly, *J. Photochem. Photobiol., B*, 1997, **40**, 91–106.

59 B. Elias and A. Kirsch-De Mesmaeker, *Coord. Chem. Rev.*, 2006, **250**, 1627–1641.

60 V. Artero, M. Chavarot-Kerlidou and M. Fontecave, *Angew. Chem., Int. Ed.*, 2011, **50**, 7238–7266.

61 N. Queyriaux, R. A. Wahyuono, J. Fize, C. Gablin, M. Wächtler, E. Martinez, D. Léonard, B. Dietzek, V. Artero and M. Chavarot-Kerlidou, *J. Phys. Chem. C*, 2017, **121**, 5891–5904.

62 C. D. Windle, H. Kumagai, M. Higashi, R. Brisse, S. Bold, B. Jousselme, M. Chavarot-Kerlidou, K. Maeda, R. Abe, O. Ishitani and V. Artero, *J. Am. Chem. Soc.*, 2019, **141**, 9593–9602.

63 B. Shan, A. Nayak, R. N. Sampaio, M. S. Eberhart, L. Troian-Gautier, M. K. Brennaman, G. J. Meyer and T. J. Meyer, *Energy Environ. Sci.*, 2018, **11**, 447–455.

64 T.-T. Li, B. Shan and T. J. Meyer, *ACS Energy Lett.*, 2019, 629–636, DOI: [10.1021/acsenergylett.8b02512](10.1021/acsenergylett.8b02512).

65 C. Bourguignon, A. Moinel, A. Huet, Y. Kervella, C. D. Windle, J. Massin, V. Artero, M. Chavarot-Kerlidou and R. Demadrille, *Adv. Energy Sustainability Res.*, 2023, **4**, 2300095.

66 D. N. Nguyen, E. Giannoudis, T. Straistari, J. Fize, M. Koepf, P. D. Tran, M. Chavarot-Kerlidou and V. Artero, *ACS Energy Lett.*, 2024, **9**, 829–834.

67 R. N. Sampaio, E. J. Piechota, L. Troian-Gautier, A. B. Maurer, K. Hu, P. A. Schauer, A. D. Blair, C. P. Berlinguette and G. J. Meyer, *Proc. Natl. Acad. Sci. U. S. A.*, 2018, **115**, 7248–7253.

68 F. H. Case and J. A. Brennan, *J. Am. Chem. Soc.*, 1959, **81**, 6297–6301.

69 R. Nasielski-Hinkens, M. Benedek-Vamos and D. Maetens, *J. Heterocycl. Chem.*, 1980, **17**, 873–876.

70 R. Nasielski-Hinkens, M. Benedek-Vamos, D. Maetens and J. Nasielski, *J. Organomet. Chem.*, 1981, **217**, 179–182.

71 B. Kohne and K. Praefcke, *Liebigs Ann. Chem.*, 1985, **1985**, 522–528.

72 D. Z. Rogers, *J. Org. Chem.*, 1986, **51**, 3904–3905.

73 K. Praefcke, B. Kohne, F. Korinth, P. Psaras, J. Nasielski, C. Verhoeven and R. Nasielski-Hinkens, *Liebigs Ann. Chem.*, 1989, **1989**, 617–621.

74 H. Masui, A. B. P. Lever and E. S. Dodsworth, *Inorg. Chem.*, 1993, **32**, 258–267.

75 R. A. Metcalfe, E. S. Dodsworth, A. B. P. Lever, W. J. Pietro and D. J. Stufkens, *Inorg. Chem.*, 1993, **32**, 3581–3582.

76 M. Ebadi and A. B. P. Lever, *Inorg. Chem.*, 1999, **38**, 467–474.

77 P. R. Auburn and A. B. P. Lever, *Inorg. Chem.*, 1990, **29**, 2551–2553.

78 R. A. Metcalfe, E. S. Dodsworth, S. S. Fielder, D. J. Stufkens, A. B. P. Lever and W. J. Pietro, *Inorg. Chem.*, 1996, **35**, 7741–7750.

79 A. Ripak, S. De Kreijger, R. N. Sampaio, C. A. Vincent, É. Cauët, I. Jabin, U. K. Tambar, B. Elias and L. Troian-Gautier, *Chem. Catal.*, 2023, 100490, DOI: [10.1016/j.checat.2022.100490](10.1016/j.checat.2022.100490).

80 M. J. Frisch, G. W. Trucks, H. B. Schlegel, G. E. Scuseria, M. A. Robb, J. R. Cheeseman, G. Scalmani, V. Barone, G. A. Petersson, H. Nakatsuji, X. Li, M. Caricato, A. Marenich, J. Bloino, B. G. Janesko, R. Gomperts, B. Mennucci, H. P. Hratchian, J. V. Ortiz, A. F. Izmaylov, J. L. Sonnenberg, D. Williams-Young, F. Ding, F. Lipparini, F. Egidi, J. Goings, B. Peng, A. Petrone,

T. Henderson, D. Ranasinghe, V. G. Zakrzewski, J. Gao, N. Rega, G. Zheng, W. Liang, M. Hada, M. Ehara, K. Toyota, R. Fukuda, J. Hasegawa, M. Ishida, T. Nakajima, Y. Honda, O. Kitao, H. Nakai, T. Vreven, K. Throssell, J. Montgomery Jr., J. E. Peralta, F. Ogliaro, M. H. Bearpark, J. J. Heyd, E. Brothers, K. N. Kudin, V. N. Staroverov, T. Keith, R. Kobayashi, J. Normand, K. Raghavachari, A. Rendell, J. C. Burant, S. S. Iyengar, J. Tomasi, M. Cossi, J. M. Millam, M. Klene, C. Adamo, R. Cammi, J. W. Ochterski, R. L. Martin, K. Morokuma, O. Farkas, J. B. Foresman and D. J. Fox, Gaussian, Inc., Wallingford CT, 2016.

81 J. Tomasi, B. Mennucci and E. Cancès, *J. Mol. Struct.: THEOCHEM*, 1999, **464**, 211–226.

82 A. D. Becke, *Phys. Rev. A*, 1988, **38**, 3098–3100.

83 C. Lee, W. Yang and R. G. Parr, *Phys. Rev. B: Condens. Matter Mater. Phys.*, 1988, **37**, 785–789.

84 B. Miehlich, A. Savin, H. Stoll and H. Preuss, *Chem. Phys. Lett.*, 1989, **157**, 200–206.

85 P. C. Hariharan and J. A. Pople, *Theor. Chim. Acta*, 1973, **28**, 213–222.

86 W. J. Hehre, R. Ditchfield and J. A. Pople, *J. Chem. Phys.*, 1972, **56**, 2257–2261.

87 F. Weigend and R. Ahlrichs, *Phys. Chem. Chem. Phys.*, 2005, **7**, 3297–3305.

88 D. Andrae, U. Häußermann, M. Dolg, H. Stoll and H. Preuß, *Theor. Chim. Acta*, 1990, **77**, 123–141.

89 R. L. Martin, *J. Chem. Phys.*, 2003, **118**, 4775–4777.

90 R. Nasielski-Hinkens and M. Benedek-Vamos, *J. Chem. Soc., Perkin Trans. 1*, 1975, 1229–1229, DOI: **10.1039/P19750001229**.

91 E. Ishow, A. Gourdon, J.-P. Launay, C. Chiorboli and F. Scandola, *Inorg. Chem.*, 1999, **38**, 1504–1510.

92 N. C. Fletcher, T. C. Robinson, A. Behrendt, J. C. Jeffery, Z. R. Reeves and M. D. Ward, *J. Chem. Soc., Dalton Trans.*, 1999, 2999–3006, DOI: **10.1039/A903556G**.

93 S. Ghumaan, B. Sarkar, S. Patra, J. van Slageren, J. Fiedler, W. Kaim and G. K. Lahiri, *Inorg. Chem.*, 2005, **44**, 3210–3214.

94 D. Sorsche, C. Pehlken, C. Baur, S. Rommel, K. Kastner, C. Streb and S. Rau, *Dalton Trans.*, 2015, **44**, 15404–15407.

95 P. Belser, A. Von Zelewsky and M. Zehnder, *Inorg. Chem.*, 1981, **20**, 3098–3103.

96 A. M. Pyle and J. K. Barton, *Inorg. Chem.*, 1987, **26**, 3820–3823.

97 V. Balzani, F. Bolletta, M. T. Gandolfi and M. Maestri, *Organic Chemistry and Theory*, 2006, pp. 1–64.

98 A. Masschelein, L. Jacquet, A. Kirsch-De Mesmaeker and J. Nasielski, *Inorg. Chem.*, 1990, **29**, 855–860.

99 R. Bevernaegie, S. A. M. Wehlin, B. Elias and L. Troian-Gautier, *ChemPhotoChem*, 2021, **5**, 217–234.

100 R. Englman and J. Jortner, *Mol. Phys.*, 1970, **18**, 145–164.

101 J. Olmsted and T. J. Meyer, *J. Phys. Chem.*, 1987, **91**, 1649–1655.

102 S. A. M. Wehlin, L. Troian-Gautier, A. B. Maurer, M. K. Brennaman and G. J. Meyer, *J. Chem. Phys.*, 2020, **153**, 054307.